A Structure Function Study of Organic Anion Transporting Polypeptide 1c1 (Oatp1c1)

A THESIS
SUBMITTED TO THE FACULTY OF THE GRADUATE SCHOOL
OF THE UNIVERSITY OF MINNESOTA
BY

Gregg Anthony Baldeshwiler

IN PARTIAL FULFILLMENT OF THE REQUIREMENTS
FOR THE DEGREE OF
MASTER OF SCIENCE

Dr. Grant W. Anderson, Dr. Jon N. Rumbley

October 2011

Acknowledgements

I would like to acknowledge both of my advisors, Grant Anderson and Jon Rumbley as well as Daniel Westholm whom have given me extensive training and advice throughout the progression of my research project. Kevin Viken also deserves acknowledgement for his training me on the use of lab equipment, as well as his aid given for carrying out laboratory procedures.

Dedication

This thesis is dedicated to my parents; Jim and Andrea Baldeshwiler for their moral and financial support.

ABSTRACT

The blood brain barrier (BBB) is impermeable to substrates that are not small lipophilic molecules. This aids in the prevention of toxins in the blood from entering the brain. However, this poses a barrier to drug delivery to the central nervous system (CNS). Transporters located on the brain barrier endothelial cells allow specific substrates to pass from the blood to the brain. One transporter located on the apical and basal side of the brain endothelial cells (BEC) is organic anion transporting polypeptide 1c1 (OATP1C1 (human), Oatp1c1 (rodent)). Oatp1c1 is a Na^+-independent, bidirectional transporter of not only organic anions, but also endogenous, exogenous and amphipathic organic compounds. In particular, Oatp1c1 is a high affinity thyroxine transporter and displays atypical transport kinetics. There is little known about the structure of Oatp1c1, but it is suggested to have 12 transmembrane spanning α-helices which form a barrel-like structure with a central putative pore. Because Oatp1c1 is a transmembrane spanning protein, it is difficult to obtain a crystal structure using current imaging techniques. Protein modeling has been used to create a probable 3-dimensional (3D) structure based on the previously crystallized structure of the glycerol-3-phosphate transporter, and homology modeling from other Oatps. We hypothesize that using homology modeling, and sequence conservation; we can target specific amino acids for mutagenesis that are thought to play a subtle role in thyroxine transport. I tested the hypothesis by making specific amino acid mutations allowing the study of Oatp1c1 dependent transport biochemistry. By determining amino acids that play a subtle role in Oatp1c1 mediated thyroxine transport, a probable structure can be further elucidated. Once the 3D structure of the protein is further elucidated and amino acids involved in transport are identified,

drugs can be rationally designed to utilize Oatp1c1 transport from the blood to the brain. In the work presented in this thesis, twelve mutations were made to further characterize the Oatp1c1 structure. Each mutation targeted an amino acid with >80% homology amongst the Oatps, except for two mutations with less than 80% homology. The targeted amino acids are proposed to be involved in substrate transport and face toward the putative substrate channel.

Wild type (WT) Oatp1c1 was fit to a biphasic profile for thyroxine transport with a K_m of 16 nM and an estimated V_{max} of 2 pmol/min/mg protein. Examination of the kinetic profiles in mutant constructs F88A, I96A, and Y227L displayed a decrease in K_m and V_{max} for thyroxine transport, as well as a conversion from biphasic to standard Michaelis-Menten kinetics when compared to WT. Kinetic profiles of mutant constructs F370A and F374A displayed higher values for K_m with similar V_{max}. These results further support the hypothesized structure for Oatp1c1 and identify key amino acids involved in substrate positioning within the putative pore. Results may also indicate the presence of non-overlapping high affinity and low affinity binding sites within Oatp1c1.

TABLE OF CONTENTS

LIST OF TABLES

LIST OF FIGURES

LIST OF ABBREVIATIONS

3D	Three Dimensional
AA	Amino Acid
ABC	ATP-Binding Cassette
ACE	Angiotensin converting enzyme
AET	Active Efflux transport
ALD	ATP-Binding Cassette, sub-family D
ATP	Adenosine-5'-triphosphate
BBB	Blood-Brain Barrier
BCA	Bicinchoninic Assay
BCRP	Breast Cancer Resistant Protein
BCSFB	Blood Cerebrospinal Fluid Barrier
BEC	Brain Endothelial Cell
BMGC	Biomedical Genomics Center
BQ-123	D-tryptamine-D-aspartic acid-L-proline-D-valine-L-leucine
BSP	Bromosulfophthalein
cAMP	Cyclic Adenosine Monophosphate
CAT	Cationinc amino acid transporter
CCK-8	Cholecystokinin
cGMP	Cyclic Guanosine Monophosphate
CHT	Choline Transporter
Cl_{int}	Free Intrinsic Clearance
CMT	Carrier mediated transport
CNS	Central Nervous System
CNT	Concentrative nucleoside transporter
CPM	Counts Per Minute
CRC 220	4-methoxy-2,3,6-trimethylphenylsulfonyl-L-aspartyl-D-4-amidinophenylalanyl-piperidide
CSF	Cerebrospinal Fluid
DHEAS	Dehydroepiandrosterone
DPDPE	[D-penicillamine2,5]-enkephalin
$E_1$3βG	Estrone 3-β-D-glucuronide
E1S	Estrone-1-Sulfate
$E_2$17βG	Estradiol-17β-glucuronide
$E_2$3βG	Estradiol-3β-glucuronide
$E_3$17βG	β-estriol 3-β-D-glucuronide
E-3-S	Estrone-3-Sulfate
ECs	Endothelial Cells

FBS	Fetal Bovine Serum
FITC	Fluorescein Isothiocyanate
FLVCR	Feline Leukemia Virus subgroup C receptor-related protein
GLUT	Glucose Transporter
GNC	GATA, nitrate-inducible, carbon metabolism-involved
hCT	Human Carnitine Transporter
HEK293	Human Embryonic Kidney Cells 293
HIAT	Hippocampus Abundant Transcript
HIV	Human Immunodeficiency Virus
hOAT	Human Organic Anion Transporter
hOCT	Human Organic Cation Transporter
hROAT	Human Renal p-Aminohippurate transporter
IHC	Immunohistochemistry
ISF	Interstitial fluid
JAMs	Junction adhesion molecules
K_m	Michaelis Constant
LAT	Large amino acid transporter
LTC4	Leukotriene C4
MCT	Monocarboxylic acid transporter
MDR	Multidrug resistance protein
MEM	Minimum Essential Media
MFS	Major Facilitator Superfamily
MFSD	Major Facilitator Superfamily domain-containing protein
MRP	Multidrug-Resistance like Protein
NAGLT	Na^+ - Dependent Glucose Transporter
NBT	Nucleobase transporter
OABP	2'-5'-oligoadenylate-binding protein
OAT	Organic anion transporter
OATP1C1	Human Organic anion transporting polypeptide 1c1
Oatp1c1	Rat Organic anion transporting polypeptide 1c1
OCTN	Organic Cation/carnitine transporter
P21G	Prednisolone 21-β-D-glucuronide
PBSA/TX100	Phosphate Buffered Saline, Bovine Serum Albumin, TritonX-100
pEF-DEST51	pEF-DEST51 Gateway Vector (Invitrogen)
PGD_2	Prostaglandin D2
PGE_1	Prostaglandin E1
PGE_2	Prostaglandin E2
$PGE_{2\alpha}$	Prostaglandin 2α

RMT	Receptor Mediated Transport
rT3	Reverse-Triiodothyronine
rT3S	Reverse T3 Sulfate
SLC	Solute Carrier
SPIN	Spindlin
SV2A	Synaptic Vesicle Glycoprotein 2A
T_2	Diiodothyronine
T_3	Triiodothyronine
T3S	T3 Sulfate
T_4	Thyroxine
T4S	T4 Sulfate
TAP	Transporter associated with Antigen Processing
TXB_2	Thromboxane
V_{MAX}	Maximum velocity of transport
WT	Wild Type

INTRODUCTION

The blood-brain barrier (BBB) has two fundamental roles: protect the brain from substances within the blood that could have potentially negative effects such as drugs, endobiotics, xenobiotics and toxins, as well as provide the brain appropriate nourishment by allowing nutrients to gain successful entry [1-2]. These tasks are done by regulating substances within the brain through the activity of small molecule transporters [3]. However, protection from contents of the blood has drawbacks when it comes to drug delivery to the central nervous system (CNS) as more than 98% of all tested neurotherapeutic candidate drugs are prevented from crossing the BBB [4].

Within the brain, there are many microvessels supplying the brain with appropriate nutrients. In addition, the choroid plexus secretes cerebrospinal fluid (CSF), which is located within the subarachnoid space and cerebral ventricles. Barriers also exist separating the blood from the cerebral spinal fluid (CSF). These barriers are necessary for the regulation of molecules crossing from the blood to the fluid spaces or neural tissue [5]. The BBB separates the blood from the brain interstitial fluid (ISF), the choroid plexus separates the blood from the ventricular CSF, and the arachnoid epithelium separates the blood from the subarachnoid CSF [5].

The brain is highly vascularized and the blood vessels are lined with specialized endothelial cells (ECs) that are strongly coupled by adherens junctions and tight junctions, as well as surrounded by astrocyte end-foot processes on the abluminal side [1, 6-7]. Brain endothelial cells are more specialized than peripheral ECs because they

contain tight junctions and there are fewer endocytotic vesicles that would allow substrates to be more easily transported [3, 6]. Astrocytes are located on the basal side of the ECs and are responsible for production of signaling molecules such as cytokines and neurotrophins [8]. For substances to enter the brain from the blood, they must first cross the luminal and abluminal membranes on the ECs, diffuse through the extracellular fluid and transport into the astrocytic foot processes, neurons, microglia, or oligodendrocytes. Together, astrocytes, pericytes, neurons, and the extracellular matrix combined with the cerebral endothelial cells make up the 'neurovascular unit.'

Tight junctions hold adjacent ECs together through the proteins claudin and occludin (similar to the connexins found in gap junctions [9]), junction adhesion molecules (JAMs) and endothelial selective adhesion molecules [1]. Claudins (3,5 and 12) and occludin, each of which contain four transmembrane domains, have large extracellular loops whose interactions tightly couple adjacent ECs, creating the BBB [1]. Because of the BBB, molecules that need to get from the blood to the brain require specific transport systems [10-12]. Due to the nature of ECs lining the microvasculature of the brain, substances must cross both the luminal and abluminal membranes which require transporters on both membranes. Molecules traveling to the brain need to overcome the BBB, while molecules traveling to the CSF must pass the blood cerebral spinal fluid barrier (BCSFB) via the choroid plexus or subarachnoid space. Due to the high vascularization and relative proximity of brain capillaries to neurons (8-20 μm), the BBB tightly controls molecule entry to the brain [1, 13].

The BBB is host to a wide variety of endogenous transporters for recognition of a vast array of substrates. Four separate mechanisms are utilized for transport at the BBB: free diffusion, simple diffusion through aqueous pores, facilitated diffusion**,** and active transport using a protein carrier (e.g. ATP). Free diffusion does not require a transmembrane transporter but instead relies on both chemical and electrical potential gradients to go through the BBB. The paucity of fenestrations makes simple diffusion of substrates through aqueous pores arduous, unless they are small, lipophilic molecules (eg. CO_2, O_2, ethanol, etc.) which can be transported passively from the blood to the brain [14]. However, BBB disruption would allow more substances to freely diffuse through aqueous gaps or spaces. In the case of trauma, multiple sclerosis and HIV, to list a few, BBB disruption may occur [15]. Facilitated diffusion passively uses a protein carrier molecule to transport substances across the cell membrane. Monocarboxylates, hexoses, amino acids, nucleosides, and small peptides are some of the examples of molecules that use facilitated diffusion for BBB transport [16].

Facilitated transport can be further characterized based on types of transport. These transporters can be classified into three separate groups: carrier-mediated transport (CMT), active efflux transport (AET), and receptor mediated transport (RMT) [17]. Carrier mediated transporters can be dependent on energy or co-transport of another molecule. Within the human CMT group are the proteins: glucose transporter 1 (GLUT1) a member of the SLC2 gene group, large amino acid transporter 1 (LAT1), cationic amino acid transporter 1 (CAT1), monocarboxylic acid transporter 1 (MCT1), concentrative nucleoside transporter (CNT2), nucleobase transporter (NBT), sodium-

dependent choline transporters (CHT), organic anion transporters (OAT), organic cation transporters (OCT) and organic anion transporting polypeptides (OATP) [17]. Carrier-mediated transport is the process by which the brain is supplied with nutrients [2].

Active efflux transporters located endogenously in the brain are ABCB1, ABCCs and ABCG2. P-glycoprotein is probably the most studied AET, and is encoded by ABCB1 or MDR1[18]. Active efflux relies on multiple transporters in series and utilizes both energy dependent and independent forms [19]

The major facilitator superfamily (MFS) is a large group of homologous 12-transmembrane transporters with 17 subfamilies that transport a wide variety of substrates. Members include uniporters, symporters, antiporters, cotransporters and are found in prokaryotic and eukaryotic organisms. Examples of human transporters included within the MFS family are FLVCR, HIAT, MFSD, NAGLT, OAT, OCTN, SLC16, SLC17, SLC18, SLC21, SLC22, SLC37, SLC43, SLC45, SLC46, SPIN, SV2A, hCT, hOAT, hOCT,and hROAT [20]. Members of the solute carrier 22 class are Na^+-dependent organic anion/cation transporters (HUGO).

Solute carrier 16 family members are Na^+-independent transporters of aromatic amino acids across the plasma membrane. SLC16A2 is the gene that represents MCT8, a monocarboxylic acid transporter that transports T4, T3, T2 and rT3 across the blood brain barrier. A notable MFS protein, glycerol-3-phosphate transporter, has 12 transmembrane spanning domains with a previously determined crystal structure. The glycerol-3-

phosphate transporter crystal structure has been used in conjunction with structures of lactose permease and multidrug resistant protein D in *Escherichia coli* as a template for *in silico* Oatp1c1 structure determination [21].

The Solute Carrier (SLC) superfamily consists of more than 300 proteins divided amongst 48 families (SLC1-48) [22]. Each SLC family represents a class of solute carriers with specific substrates, homology, and characteristics of transport. SLC21, 22, and 16 are located on the blood brain barrier [23]. SLC21 is the solute carrier family 21 (SLCO) which represents a broad group of solute carrier organic anion transporting polypeptides that display Na^+-independent transport [23-24]. The Organic anion transporting polypeptide (OATP human; Oatp other species) superfamily, encoded by SLCO genes, consists of multispecific sodium-independent transport proteins that show a vast array of tissue expression [23]. Members of this family are distinguished by homology, tissue distribution and substrate recognition. Mammalian OATPs/Oatps with more than 40% amino acid identity are grouped within the same family (OATP1, OATP2, OATP3, OATP4, OATP5 and OATP6) and proteins with more than 60% identity are grouped within the same subfamily (OATP1A, OATP1B, and OATP1C) [24]. Within the human genome, there are 11 SLCO genes: 1A2, 1B1, 1B3, 1C1, 2A1, 2B1, 3A1, 4A1, 4C1, 5A1, and 6A1. Genes included within rodents consist of the previous 11, as well as 1a1, 1a3, 1a4, 1a5, 1a6, 1b2, 6b1, 6c1 and 6d1. Thyroid hormone transporters associated with the SLCO genes are: SLCO1A2, SLCO1B1, SLCO1B3, SLCO1C1, SLCO4A1 and SLCO4C1 [25-29]. Below is a summary of what is known

about localization, substrates, and polymorphisms occurring within the human OATPs expressed in brain barrier cells.

OATP1A2 (SLCO1A2)

The protein translated by SLCO1A2 is OATP1A2, a transporter that is 670 amino acids long, within the human liver and brain [30]. SLCO1A2 is located on chromosome 12p12 [23]. There is 67% amino acid identity when OATP1A2 is compared to rat Oatp1a1 [30]. Substrates recognized by OATP1A2 include, but are not limited to, Deltorphin II, microcystin, DHEAS, estrone-3-sulfate, Estradiol-17β-glucuronide, DPDPE, T_3, T_4, fexofenadine, ADP-ajmalinium, rocuronium, microcystin-LR, bromosulphthalein, bile acids, steroid sulfates, organic cations, opioid peptides, levofloxacin, pitavastatin, rosuvastatin, saquinavir [26, 30-41]. OATP1A2 has low affinity toward T_4 (K_m = 8 μM) suggesting the need for a high thyroid hormone concentration for transport in the brain possibly indicating a role as an alternative transporter for thyroid hormone [25]. Tissue distribution include: protein found in brain (BBB) and liver, and mRNA found in kidney, lung and testes [30-31]. Ethnicity is the distinguishing factor for allelic frequency, which ranges from 1-11% based on the single nucleotide polymorphisms described by Lee et al [36]. Allele frequency for most SLCO1A2 polymorphisms within Caucasians is <1% [36, 42]. Some of the polymorphisms- T38C (I13T), A516C (E172D), R168C and N278X display altered transport function of methotrexate disposition and response [42]. Transport reduction was noticed for estrone sulfate (E1S) and deltorphin II for variants E172D (predicted location is within the fourth transmembrane α-helix) and A404T (N135I) (predicted location is in the extracellular domain) [36]. SLCO1A2

polymorphisms G559A (A187T) and C2003G (T668S) have substrate dependent changes in transport activity [36]. In a study by Van der Deure, examination of I13T (located on the cytoplasmic side) and E172D polymorphisms displayed T_3 serum levels higher and equal to WT respectively [43]. Predicted to be located extracellularly between the third and fourth α-helix and found only in African Americans with allelic frequency of 1%, polymorphism A382T (N128Y) had lower uptake of estrone sulfate, deltorphin II, and [D-penicillamine2,5] enkephalin (DPDPE) than WT SLCO1A2 [36].

OATP1C1/Oatp1c1 (SLCO1C1/ slco1c1)

The gene encoding Oatp1c1 is located in on chromosome 12p12 and is the only member of the Oatp1c class in humans and rodents [24]. Protein expression of Oatp1c1 has been found in the luminal and abluminal membranes of BBB endothelial cells, the basolateral membrane of choroid plexus epithelial cells, human ciliary body epithelial cells, and Leydig cells of the testes [44-46]. Oatp1c1 is a plasma membrane localized, Na^+-independent, bi-directional transporter of, not only anionic compounds as the name would imply, but amphipathic compounds across the BBB [45, 47-48]. Substrates recognized and transported by the 716 amino acid long, rat Oatp1c1 protein include: bromosulfophthalein, T_4, rT_3, estradiol-17β-glucuronide, estrone-3-sulfate, cerivastatin, troglitazone-sulfate, taurocholate and digoxin and has been cloned with a V5 epitope and 6x His tag on the C-terminus [28, 49-52]. The human OATP1C1 transporter consists of 712 amino acids. Inhibitors of Oatp1c1-dependent T_4 and $E_2$17βG transport include multiple sterol glucuronides such as: $E_3$17βG, P21G, $E_1$3βG, estrone 3-β-D-glucuronide,

$E_2$3βG, dehydroepiandrosterone 3-glucuronide [53]. Measured K_m of T_4 transport has varied amongst studies- ranging from 90-340 nM [28, 45-46].

Atypical kinetic profiles are defined by their deviance from standard Michaelis-Menten kinetics and the possible incorporation of multiple binding sites. Oatp1c1 has been previously determined to display atypical kinetics, with Oatp1c1 mediated transport of T_4 and $E_2$17βG both demonstrating biphasic kinetics [53]. Previous self and *cis*-inhibition studies have been used to determine if T_4 and $E_2$17βG interact with the same Oatp1c1 binding sites [53]. Because the K_i for unlabeled T_4 and $E_2$17βG inhibition of $^{125}T_4$ was not equal to the K_i for unlabeled $E_2$17βG and T_4 inhibition of ^{3}H- $E_2$17βG it was determined that T_4 and $E_2$17βG recognize Oatp1c1 binding sites differently [53]. Based on competitive inhibition studies and dose response curves, Westholm et al. has also determined that T_4 and $E_2$17βG recognize the same Oatp1c1 binding sites, but with opposite affinities (K_m = 10.3 nM, Cl_{int} = 4.2 μL/min/mg protein and K_m = 22.0 μM, Cl_{int} = 0.5 μL/min/mg respectively, where Cl_{int} is the measure of clearance mediated solely by the low affinity binding site) [53]. Multiple OATPs have been identified as having multiple binding sites dependent on; type of substrate, pH gradients, or substrate concentration. OATP1B1 has also been shown by multiple groups to display biphasic kinetics in the presence of the substrate estrone-3-sulfate [54-55]. There is also evidence supporting multiple binding sites associated with OATP2B1, OATP1B3, Oatp1a4 and Oatp1c1 [52-53, 56-57]. Based on the amount and variation of substrates transported by

the OATP family, it is probable that more OATPs will display atypical kinetics upon further investigation. This study will examine the kinetics of T_4 transport for Oatp1c1. A crystal structure has yet to be obtained for any OATP/Oatp. All Oatps have 12 predicted transmembrane spanning domains and a large extracellular loop between transmembrane domains 9 and 10 [23]. This extracellular loop houses many conserved cysteines which display similarity to zinc-finger domains of transcription factors [58]. Structural predictions are based on homology modeling to previously crystallized structures; glycerol 3-phosphate transporter, lactose permease, and the multidrug transporter *Escherichia coli* multidrug resistance protein D as templates [21]. Few studies have been done to identify amino acids important for substrate recognition and transport. With a lack of available crystal structure, one must resort to an *in silico* approach for model generation. Once a model has been created, site directed mutagenesis can be utilized to target specific amino acids potentially involved in substrate recognition.

Mutations previously analyzed based on sequence conservation and structural orientation include: D85A, E89A, N92A, R601S, P609A, W277A/W278A, W277F/W278F, G399A/G409A, and G399V/G409V [21]. These mutations were chosen because of the high impact on substrate transport. Positively charged amino acids were mutated to neutral or negatively charged amino acids to annihilate negatively charged substrate recognition. This type of study has relevance in Oatp1c1 structure determination by predicting amino acid direction within the putative pore necessary for substrate transport.

It was found that mutations in transmembrane domain 2 (D85A, E89A, N92A) show increased intracellular localization, and no uptake of ^{125}I-T_4 above empty vector. Screening of double mutations G399/409A, G399/409V (transmembrane 8), and single mutations R601S, P609A (transmembrane 11) each decrease ^{125}I-T_4 uptake at 10 minute time points [21]. Kinetic profiling suggests double mutation W277F/W278F and single mutations R601S and P609A maintain the biphasic curve fit, while double mutations G399A/G409A, G399V/G409V knock out the low affinity binding site [21].

Possibly the most important findings by Westholm et al. show that the double mutation to TM6 residues W277A/W278A completely abolished T_4 transport [21]. This could be indicative of the role of tryptophan as a protein anchor on the periplasmic side, as well as an indicator that in *silico* analysis was correct in the prediction of orientation and direction of TM6. According to Schiffer et al. tryptophan residues are not randomly distributed- they occur at the surface of a cell to form hydrogen bonds with the lipid head groups while the hydrophobic rings are found in the lipid part of the bilayer [59]. Co-mutation of W227F/W278F of TM6 still gave rise to biphasic kinetics, but there was a 10-fold increase in high affinity K_m for T_4 transport [21]. For transmembrane domain 8, a double glycine to alanine (G399A/G409A) mutation resulted in protein localization to the plasma membrane with diminished transport at high concentrations [21]. Diminished T_4 transport could be the result of disabling free rotation of about the phi and psi angles of glycine or the disruption of helix-helix contact points afforded by glycine with its lack of a side chain. The same trend occurred with the co-mutation G399L/G409L [21]. Mutations made to transmembrane domain 11 (R601S and P609A) show partial

thyroxine transport with significantly reduced V_{max}, and elevated K_m [21]. These findings are possibly due to the mutation of a positive, pore facing amino acid, to a small polar molecule such as serine as in the case of R601S. It is thought that the negative electrostatic potential found within many Oatp substrates uses the positively charged arginine as a recognition site before passing through the protein. Transmembrane domain 11 also houses proline 609, which was mutated to an alanine in a previous study [21]. Thyroxine transport was significantly diminished in the P609A mutant that may be related to the increased cellular trapping of expressed protein. However, the high affinity K_m associated with P609A was 20-times higher than WT at 42 nM, suggestive of a role for this proline in thyroxine recognition [21].

There is little known about the structure of Oatp1c1, but it is suggested to have 12 transmembrane spanning α-helices that form a barrel-like structure with a central putative pore [60]. Due to Oatp1c1 spanning the plasma membrane, the crystal structure is difficult to obtain. Protein modeling has been used to create a probable 3-dimensional structure based on the previously crystallized structure of glycerol-3-phosphate, and homology modeling from other Oatps that contains a highly conserved arginine thought to be involved in substrate transport. WT Oatp1c1 demonstrates atypical kinetics and may contain two binding sites- one high affinity and one low affinity. These two binding sites may be independent or partially overlap. Making specific amino acid mutations will allow us to study the effect on kinetics of Oatp1c1 dependent transport of thyroxine (T_4). By finding which amino acids are essential for Oatp1c1 mediated thyroxine transport, the structure can be further elucidated. Once the 3D structure of the protein is determined, as

well as amino acids important for transport, drugs can be rationally designed to utilize Oatp1c1 transport from the blood to the brain.

In the studies described in this thesis, twelve mutations were made to further characterize Oatp1c1 structure: F88A, F88L, I96A, I96S, Y227A, F243A, F243L, Q365A, F370A, F370L, F374A, and F374L. Each of these mutations targeted an amino acid with >80% homology amongst the Oatps, indicative of the evolutionary importance. The targeted amino acids are thought to be involved in substrate transport and face toward the putative protein channel while the mutations were designed to have little impact on structure but based more on steric constraints. Phenylalanine (F) is a nonpolar amino acid with a large, aromatic, side chain which was targeted due to the steric constraints it ensues upon substrate transport as well as the stacking interactions involving Van Der Waals forces within the protein. Isoleucine (I) is a nonpolar amino acid with a long, aliphatic, hydrophobic side chain that may be involved in the recognition and transport of hydrophobic ligands. Amino acid mutations to alanine (A) were made to ease the large steric constraints associated with larger side chains.

Oatp1c1 is important for BBB transport but many aspects remain unknown about structure, molecular recognition, and mechanism of transport. Targeting amino acids for site directed mutagenesis will further our knowledge on Oatp1c1 structure while expanding the current understanding of amino acids required for Oatp1c1 mediated thyroxine transport. With structural characterization of Oatp1c1, novel compounds can be developed for efficient transport across the blood brain barrier.

METHODS

Creating Oatp1c1 mutant constructs

Oatp1c1 was cloned into pEF-DEST51 expression vector according to Westholm et al [50]. based on the protocol by Hartley et al [61]. Oatp1c1-pEF-DEST51 expression vector was used to transform DH5α™ competent cells using MAX efficiency® DH5α™ competent cell protocol (Invitrogen™ corp, Carlsbad, CA). Empty vector (pEF-DEST51) plasmid DNA was transformed into DB3.1 competent cells (Invitrogen™ corp, Carlsbad, CA). Briefly, competent cells were thawed on ice, 100 µL was aliquoted into a chilled 14 mL polypropylene tube and 10 ng of Oatp1c1-pEF-DEST51 DNA was added and incubated on ice for 30 min. Cells were then heat shocked for 45 seconds at 42^0 C in a water bath then placed on ice for 2 min and 900 µL of SOC medium was added. Incubation was performed for 1 hour in a 37^0 C incubator with shaking at 225 rpm. The reaction was then diluted 1:10 in SOC medium and plated on LB plates containing 50 µg/mL ampicillin and incubated overnight at 37^0 C. Plasmid DNA was isolated using a plasmid mini- or midi-prep kit (Qiagen, Gaithersburg, MD). Once the Oatp1c1-pEF-DEST51 plasmid DNA was isolated, primers were designed to insert point mutations to alter a single amino acid as well as introduce a cryptic cut site.

The protocol was carried out according to the QuikChange® II XL site-directed mutagenesis kit using XL10-Gold® ultracompetent cells (Stratagene, La Jolla, CA). Primers were designed using QuikChange® primer design program (Stratagene, La Jolla, CA). Mutations were screened by digestion with varying restriction endonucleases, dependent upon cryptic cut site insertion, and run on a DNA agarose gel by

electrophoresis then further verified by sequencing at the University of Minnesota Biomedical Genomics Center (BMGC). Single amino acid mutations were designed based on the original Oatp1c1 cDNA sequence. A genomic mapping program (GMAP) was used to identify restriction sites within each of the mutant Oatp1c1 constructs which would introduce a translationally silent restriction site as seen in Table 1. Vector features and restriction digest maps are depicted in Figure 1.

Transfection

Electroporation

HEK293 cells were grown to 50-70% confluence on a 10 cm plate coated with rat tail collagen (Gibco by Invitrogen, Carlsbad, CA). Growth media (MEM) containing fetal bovine serum (10% v/v), sodium pyruvate (10 mM), non-essential amino acids (10 mM), and penicillin/streptomycin (100 U/mL) was aspirated off. The cells were then washed with 5 ml of phosphate buffered saline. Two mL of 0.25% Trypsin-EDTA (Invitrogen™ corp, Carlsbad, CA) was added and the cells were incubated in a CO_2 containing incubator at 37^0 C until the cells detached. Trypsin-EDTA was neutralized using 8 mL of MEM containing fetal bovine serum (10% v/v), sodium pyruvate (10 mM), and non-essential amino acids (10 mM) without antibiotics. Cells were then centrifuged at 500 x g for six minutes at room temperature to obtain a cell pellet. Media was aspirated off and homogenously resuspended in MEM containing sodium pyruvate (10 mM) and non-essential amino acids (10 mM) to a density of 2.5×10^6 cells/mL. An electroporator (BIO RAD) was used with parameters set to: square wave pulse, 25 msec pulse length, and 240V using a 0.4 cm cuvette and 400 µL cell volume. Plasmid DNA was added at a final

concentration of 20 µg/mL and cells suspended at 2.5 x 10^6 cells/mL were added to a final volume of 400 µL. After a single pulse in the shockpod, cells were plated at 3.0 x 10^5 cells/well in 500 µL of growth media without antibiotics. Plates were gently rocked to obtain even distribution and incubated 24-48 hours in a 37^0 C, 5% CO_2 incubator with 95% relative humidity. Maintenance of HEK293 cells was done using growth medium containing fetal bovine serum (10% v/v), sodium pyruvate (10 mM), non-essential amino acids (10 mM), and penicillin/streptomycin (100X).

FuGENE HD Transfection reagent

HEK293 cells were grown to 70% confluence on a Falcon 24-well plate coated with rat tail collagen and the FuGENE HD transfection protocol was followed and optimized for pcDNA3.1 GFP (Roche Applied Science, Mannheim, Germany). Briefly, media and reagents were adjusted to room temperature, FuGENE HD transfection reagent was vortexed for one second, and plasmid DNA was diluted in MEM containing fetal bovine serum (10% v/v), sodium pyruvate (10 mM), and non-essential amino acids (10 mM) to a concentration of 0.02 µg/µL. A 3:2 ratio of FuGENE to DNA was used and mixed vigorously for 2 seconds. The mixture was then incubated at room temperature for 15 minutes and 25 µL of the transfection complex was added below the media surface to the adherent HEK293 cells and incubated 48 hours in a 37^0 C incubator with 5% CO_2 and 95% relative humidity. Maintenance of HEK293 cells was done using growth medium containing fetal bovine serum (10% v/v), sodium pyruvate (10 mM), non-essential amino acids (10 mM), and penicillin/streptomycin (100X).

Lipofectamine 2000

Transient transfection of Oatp1c1 was also performed using the plasmid DNA transfection method described in the Lipofectamine™ 2000 insert (Invitrogen™ corp, Carlsbad, CA). Cells were plated at 1.5 x 10^5 cells in 500 µL of complete media: MEM containing fetal bovine serum (10% v/v), sodium pyruvate (10 mM), and non-essential amino acids (10 mM) without antibiotics, on a 24-well plate, and incubated overnight to reach 95% confluence. Plasmid DNA (0.8 µg) was diluted to 50 µL in Opti-MEM I reduced serum media (Invitrogen™ corp, Carlsbad, CA), containing no serum, and gently mixed. Lipofectamine 2000 (2.0 µL) was diluted to 50 µL in opti-MEM I reduced serum media (Invitrogen™ corp, Carlsbad, CA), containing no serum, gently mixed and incubated for 5 minutes at room temperature. After the 5 minute incubation, diluted plasmid DNA and Lipofectamine were mixed to a final volume of 100 µL and the mixture was incubated for 20 minutes at room temperature. 100 µL of complex was added to each well containing cells and medium. Cells were placed into a 37^0C incubator with 5% CO_2. After being in the incubator for 4-6 hours the cells were removed and the media was changed to complete media containing fetal bovine serum (10% v/v), sodium pyruvate (10 mM), and non-essential amino acids (10 mM) without antibiotics. Maintenance of HEK293 cells was done using growth medium containing fetal bovine serum (10% v/v), sodium pyruvate (10 mM), non-essential amino acids (10 mM), and penicillin/streptomycin (100X).

Stable transfection of Oatp1c1-pEF-DEST51 mutants in Human Embryonic Kidney (HEK) 293 cells

HEK293 cells were plated at $1.2x10^5$ cells/ well to a 24-well plate in complete media containing fetal bovine serum (10% v/v), sodium pyruvate (10 mM), and non-essential amino acids (10 mM) without antibiotics and grown to >95% confluence. Cells were transfected with linearized F88A, F374A, F370A, Y227L, or I96A Oatp1c1 mutated plasmid DNA using Lipofectamine 2000 (Invitrogen™ corp, Carlsbad, CA) on 24-well BD Falcon cell culture plates (BD Biosciences, Franklin Lakes, NJ) coated with rat tail collagen (Gibco by Invitrogen, Carlsbad, CA). Five hours after transfection, media was changed to complete media containing FBS (10% v/v), sodium pyruvate (10 mM), and non-essential amino acids (10 mM) without antibiotics and placed in 37^0 C incubator with 5% CO_2 for 45 hours. Following incubation, media was changed to complete media containing fetal bovine serum (10% v/v), sodium pyruvate (10 mM), non-essential amino acids (10 mM), penicillin/streptomycin (100X), and blasticidin (10 mg/mL). Cells were grown under the pressure of blasticidin (10 mg/mL) on the 24-well plate for 7 days. Media was changed every 24-36 hours to remove dead cells and supply fresh nutrients. When cells reached >95% confluence, they were trypsinized and plated on 10-cm cell culture plates at 1:10 dilution in fresh stably transfected cell growth media containing blasticidin (10 mg/mL). Once >95% confluence was obtained on the 10 cm cell culture plate, cells were passaged at 1:10 four more times before use.

Immunohistochemistry

HEK293 cells were grown on glass coverslips coated with 5 mg/cm^2 poly-D-Lysine hydrobromide (cat number 354210, BD Biosciences, Bedford, MA). At 95% confluence, cells were transiently transfected with Lipofectamine 2000 and incubated for 48 hours at

37^0 C with 5% CO_2. Coverslips with attached cells were washed with PBS, dunked in room temperature methanol, and transferred to a new 24-well plate containing methanol at -20^0 C and fixed for up to 24 hours. Coverslips were removed from methanol and washed with PBSA/TX100 (Phosphate buffered saline (PBS), BSA (1% w/v), TritonX-100 (0.1 % v/v) three times for 5 minutes. Mouse anti-V5 antibody (Invitrogen Corporation, Carlsbad, CA) was diluted to 10 μg/mL and added to cell coated coverslips at 0.26 mg/cm^2 and incubated in a 37^0 C humidity chamber for 1 hour. Following incubation coverslips were washed 3 times for 5 minutes with PBSA/TX100. Goat anti-mouse IgG with conjugated fluorescein isothiocyanate (FITC) (Invitrogen) was spiked with Hoechst 33342 (Invitrogen), added to the coverslips, incubated in a 37^0 C humidity chamber for 1 hour and washed 3 times for 5 minutes with PBSA/TX100. Coverslips were then partially dried and mounted using ProLong Antifade kit (Invitrogen).

Transport Assays

Transiently or stably transfected cells were plated at 2.5 x 10^5 cells/well on 24-well Falcon cell culture plates in standard growth media as described above. Twenty four hours prior to the assay cells were given fresh assay media supplemented with 10 mM sodium butyrate and 10% stripped FBS. Cells were first washed with Krebs-Henseleit buffer [142mM NaCl, 23.8mM $NaHCO_3$, 12.5 mM HEPES, 5 mM glucose, 4.83 mM KCl, 1.53 mM $CaCl_2$, 1.2 mM $MgSO_4$, and 0.96mM KH_2PO_4 (pH 7.4)] and equilibrated for 10 minutes at room temperature. Buffer was removed and cells were exposed to 200 μL of 1nM L-[^{125}I]-Thyroxine (Perkin Elmer Inc., Boston, MA) diluted in Krebs-Henseleit with, unlabeled L-thyroxine added for concentrations over above 1 nM, and

incubated at room temperature. Following incubation, cells were washed twice with ~330 μL of Krebs-Henseleit buffer. Cells were then lysed with 0.5% TritonX-100 (Sigma; St. Louis, MO) and the radioactivity measured using a 2470 Wizard gamma counter (Perkin Elmer Inc., Boston, MA). Protein concentration was determined using a bicinchoninic assay (BCA) (Pierce; Rockford, IL). Counts were divided by total protein to account for expression. Oatp1c1 mutant containing constructs' counts were multiplied by radiolabeled:nonradiolabeled ratio to correct for nonradiolabeled isotope.

Calculations and Statistical analysis

Calculating ^{125}I-T$_4$ velocity

Gamma activity was determined using 2470 Wizard gamma counter (Perkin Elmer Inc., Boston, MA). Analyzing mutant uptake consisted of dividing counts per minute (CPM) by milligrams of total protein (CPM/mg) and subtracting empty vector counterpart CPM/mg. Conversion of CPM/mg to velocity (nmol/mg/min) was achieved as follows: a specified volume of 1 nM L-[^{125}I]-thyroxine was counted to determine specific activity in CPM/μL/nM, CPM of samples were multiplied by 10^{-6}, divided by CPM/μL/nM and divided by corresponding time. Correction of CPM for radiolabeled:non-radiolabeled isotope were multiplied by the dilution factor. An example equation for unit conversion is shown below.

$$Velocity = \frac{CPM}{mg\ protein}\ x\ \frac{1\ \mu L}{CPM}\ x\ \frac{10^{-6}\ L}{1\ \mu L}\ x\ \frac{1\ nmol}{1\ L}\ x\ \frac{1}{min} = \frac{\frac{nmol}{min}}{mg\ protein}$$

Two-way ANOVA with Bonferroni post test was carried out to determine difference in mutant versus empty vector uptake during screening process using GraphPad Prism 5.02 for Windows, GraphPad Software, San Diego California USA.

Nonlinear regression was used for K_m and V_{max} determination based on the equation $Y = (V_{max} * [S])/ (K_m + [S])$, where Y is velocity (pmol/min/mg), V_{max} is maximum velocity of transport (pmol/min/mg protein), [S] is T_4 concentration (nM) and K_m is the Michaelis constant (nM). Michaelis constant and maximum enzyme velocities were calculated based on least squares analysis fit within the Prism software. Wild type Oatp1c1 was fit to biphasic uptake using the equation $Y = [(V_{max} * [S]) + (Cl_{int} * [S]^2)]/ (K_m + [S])$, where Cl_{int} is the slope of the curve after the high affinity binding site has reached saturation. Michaelis-Menten constant, maximum velocity of transport and free intrinsic clearance are calculated based on least squares analysis curve fit within Prism.

RESULTS

Oatp1c1 was successfully cloned into pEF-DEST51 expression vector and transformed into XL-10 Gold or DH5α competent cells. Growing colonies, expressing ampicillin resistance, were picked and submitted to plasmid DNA extraction via mini- or midi- prep (Qiagen, Gaithersburg, MD or Invitrogen corp, Carlsbad, CA). Primers (Table 1) were used to insert point mutations and cryptic cut sites to the WT Oatp1c1 gene (Fig. 1). Mutations demonstrated expected banding patterns (Fig. 2) when analyzed by restriction digest and run on agarose gels (Fig. 3). Final verification was done by DNA sequence analysis at the University of Minnesota Biomedical Genomic Center (BMGC).

Amino acids targeted for mutation were based on side chain structure in which the side chain volume was decreased (Fig. 4). Figure 5 shows the predicted 12 transmembrane domains and amino acid conservation throughout the Oatps where the N- and C- termini lie on the intracellular side. Sequence alignment comparing Oatp1c1 and other rat Oatps shows that α-helix 2 has the highest conservation (Fig. 5), and upon closer inspection phe88 and iso96 conservation can be seen throughout the rat Oatp sequences (Fig. 6). Homology mapping was used to align Oatp1c1 to a structure containing 12 transmembrane domains surrounding a central putative pore (Fig. 7 and 8).

Oatp1c1-transiently transfected HEK293 cells displayed a two to four-fold increase in ^{125}I-T_4 uptake at 10 minutes (nmol/mg total protein) when compared to mock (pEF-DEST51) transfected cells (Fig. 9 and 10). Oatp1c1 expression is predominantly localized to the plasma membrane based on IHC data (Fig. 11). Stable transfection of

HEK293 cells with WT Oatp1c1 shows four times greater uptake than empty vector at 5 minutes (Fig. 12). Using a 60 minute time course assay, WT Oatp1c1 displayed equilibrium at approximately 1400 fmol/mg protein, four times greater than empty vector transfected cells (Fig. 13). Following the time course assays, kinetic assays were used to determine Michaelis constants for Oatp1c1 WT and mutants (Fig. 14).

It is hypothesized that two binding sites contribute to the transport of T4 for WT Oatp1c1- a high affinity binding site at low concentrations (<100 nM), and a low affinity binding site at concentrations greater than 100 nM which takes over when the high affinity binding site is saturated [53]. Figure 15A shows the biphasic kinetic profile of WT Oatp1c1 with concentrations ranging from 0.1-400 nM T_4. The high affinity binding site becomes saturated at 100 nM and a second, low affinity binding site takes over to increase substrate transport by gradually increasing velocity (Fig. 15) agreeing with previous findings [53]. When analyzed by Prism 5.0 and fit to the biphasic uptake equation, WT Oatp1c1 has a $K_m = 13 \pm 3$ nM (95% CI is 6.5-20.0 nM), and estimated $V_{max} = 1.7 \pm 0.1$ pmol/min/mg protein of the high affinity binding site ($R^2 = 0.96$) (Fig. 15). The high affinity binding site becomes saturated at 76 nM T_4 and displays standard Michaelis kinetics with $K_m = 16 \pm 1$ nM, $V_{max} = 1.9 \pm 0.0$ pmol/min/mg protein. Calculations were based on the total protein present, and it should be noted that Oatp1c1 protein concentration was not measured directly.

Reproducibility of experiments on stably transfected HEK293 cells containing Oatp1c1 mutant constructs remained consistent at concentrations from 0.1-76 nM T_4, but

variability at higher concentrations (i.e. >100 nM) led to neglecting these values during analysis, except for WT, I96A and F88L (Fig. 15). Therefore, comparisons between WT and Oatp1c1 mutant constructs were carried out based on the concentrations from 0.1-76 nM T_4.). Following is a summary of mutation effects based on α-helix number (Fig. 5).

Mutations targeting transmembrane α-helix 2 consisted of F88A/L and I96A/S (Fig. 5). Upon transient transfection of HEK293 cells, ten minute ^{125}I-T_4 uptake by mutant constructs- F88A and I96A had greater uptake than empty vector, but less than WT (Fig. 9 and 10 respectively), F88L and I96S display uptake equivalent to empty vector (Fig. 9). Examination of immunohistochemistry (IHC) staining suggest transiently transfected Oatp1c1 mutant constructs F88A/L and I96A/S have positive cellular expression, and localization predominantly on the plasma membrane. Oatp1c1 mutant construct F88L displays slight intracellular localization, as well as plasma membrane localization. No further analysis was done on mutant constructs F88L or I96S due to lack of substrate uptake (Fig. 9). Oatp1c1 mutant constructs F88A, and I96A were stably transfected into HEK293 cells for further analysis. Full time courses were carried out at room temperature to determine the linear range of ^{125}I-T_4 uptake by Oatp1c1 mutant constructs F88A and I96A. At equilibrium, ^{125}I-T_4 uptake is less than WT and greater than empty vector for stably transfected HEK293 cells with Oatp1c1 mutant constructs F88A and I96A (Fig. 13A-C). A six-minute time point was chosen, within the linear range of ^{125}I-T_4 uptake, for velocity vs. concentration (0.1-400 nM) kinetic determination (Fig. 15B and C). Oatp1c1 mutant constructs F88A and I96A displayed standard Michaelis-Menten kinetics by analyzing 0.1-76 nM T_4 with K_m of 9 ± 3 nM, V_{max} = 0.9 ± .1 (pmol/min/mg

protein), $R^2 = 0.92$ (Fig. 14C) and K_m of 12 ± 5 nM, V_{max} = 0.4 ± 0.1 pmol/min/mg protein, $R^2 = 0.85$ (Fig. 14B) respectively. Full concentration profiles (i.e. 0.1-400 nM) were generated for mutant constructs I96A and F88A displaying the loss of the low affinity binding site (Fig. 15).

Transmembrane α-helix 5 was the second target of mutagenesis. Oatp1c1 targeted mutations Y227A/L and F243A/L are found within helix 5. Tyrosine 227 is located on the intracellular side of the plasma membrane at the beginning of the helix, while phenylalanine 243 is more centralized, half-way between the intra- and extracellular space, facing the putative pore (Fig. 5, 7-8). When transiently transfected into HEK293 cells, ^{125}I-T_4 uptake at 10 minutes indicates mutant construct Y227A is slightly greater than empty (Fig. 9), while F243A (Fig. 10), and F243L (not pictured) are equal to their empty counterpart and Y227L is equal to WT (Fig. 10). When examined with IHC under confocal microscopy, mutant construct Y227A had positive expression, but localization primarily in the cytoplasm with some punctate membrane localization and Y227L showed expression with mixed localization, some intracellular, but mostly to the plasma membrane. Mutant construct F243A expression displayed predominant plasma membrane localization, while F243L was not expressed. Oatp1c1 mutant construct Y227L was stably transfected into HEK293 cells and a full time course was performed. When equilibrium was reached, mutant construct Y227L displayed greater ^{125}I-T_4 uptake than WT. Again, six minutes was chosen as the necessary time point to create a kinetic profile with ^{125}I-T_4 concentrations ranging from 0.1-76 nM. Mutant construct Y227L displayed normal Michaelis-Menten kinetics with calculated K_m = 8 ± 1.3 nM, V_{max} = 1.3

± 0.1 and R^2 = 0.97 (Fig. 14D). Oatp1c1 mutant constructs Y227A, F243A and F243L were not analyzed further.

Locations of amino acids phenylalanine 370 and 374 resided within α helix number 7. Phenylalanine 370 is located centrally within the transmembrane domain while phenylalanine 374 is located close to the extracellular side. Mutations made to Oatp1c1 for these amino acids were, F370A/L and F374A/L. Initial screening of mutant constructs F370A, F370L, F374A and F374L showed ^{125}I-T_4 uptake: equivalent to WT, equivalent to empty vector, between WT and empty vector, and equivalent to empty vector respectively (Fig. 9). Immunohistochemistry staining revealed mutant construct F370A had mixed expression between the cytoplasm and plasma membrane with most localization in the plasma membrane (Fig. 11). Positive expression was displayed by neither Oatp1c1 mutant construct F370L nor F374L, therefore, halting further analysis (not pictured). Oatp1c1 mutant construct F374A showed positive protein expression and localization to the plasma membrane (Fig. 11). Stable transfection of Oatp1c1 mutant constructs F370A and F374A into HEK293 cells was performed for further examination. Screening of Oatp1c1 mutant constructs stably transfected into HEK293 cells showed ^{125}I-T_4 uptake greater than empty vector at 5 minutes (Fig. 12). Time course evaluation, at equilibrium, shows greater ^{125}I-T_4 uptake by Oatp1c1 mutant construct F370A than WT, and ^{125}I-T_4 uptake by Oatp1c1 mutant construct F374A less than WT (Fig. 13E,F) agreeing with the five minute ^{125}I-T_4 uptake screen in Fig. 12. Velocity (pmol/min/mg protein) was plotted against ^{125}I-T_4 concentration (0.1-76 nM) for Michaelis-Menten constant determination in HEK293 cells stably transfected with Oatp1c1 mutant

constructs F370A and F374A. Assay analysis showed standard Michaelis-Menten kinetics for both mutant constructs. Oatp1c1 mutant constructs F370A and F374A (K_m = 17 ± 2 nM, V_{max} = 1.8 ± 0.1 pmol/min/mg protein, R^2 = 0.99 and K_m = 25 ± 4 nM, V_{max} = 1.5 ± 0.1 pmol/min/mg protein, R^2 = 0.97 respectively) had K_m greater than WT at room temperature (Fig. 14E and F). Overlap of standard error between WT and Oatp1c1 mutant construct F370A indicate no difference in ^{125}I-T_4 uptake (Fig. 14A and E).

DISCUSSION

Oatps are a diverse group of transporters, dispersed throughout the body, that transport a vast array of substrates [23]. Oatp1c1 is a high affinity thyroxine transporter located at the apical and basolateral membranes of brain endothelial cells, and once characterized, could serve as a target for novel drug synthesis and delivery to the CNS [45]. Among the Oatps that transport thyroid hormones are: Oatp1a2, Oatp1b1, Oatp1b3, Oatp4a1, Oatp4c1, and Oatp1c1 [25-29]. Oatp1a2 is a low affinity thyroxine transporter that may serve as a back-up to the high affinity thyroxine transporter, Oatp1c1, at the BBB. Little is known about the structure of Oatp1c1 or the amino acids involved in substrate recognition. *In silico* analysis and evolutionary conservation amongst Oatps predict 9-12 transmembrane spanning domains [21, 60]. A characteristic shared by Oatps is the positive surface potential lining the putative pore. One of the suggested amino acids involved in substrate recognition for Oatp1c1 is arginine 601, a highly conserved amino acid found throughout the Oatp class and located centrally within the putative pore [21]. The aim of this study is to identify additional critical amino acids for thyroxine transport, as well as characterize the 3D structure of Oatp1c1 further.

Pharmacophore modeling of other Oatps suggests that a substrate must have an electrostatic end with hydrogen bonding potential. This is in agreement with existing substrates, such as $E_2$17βG, taurocholate, BSP, PFOS, PFOA and thyroxine. The negative electrostatic potential of substrates is necessary for recognition by Oatp1c1 which suggests the presence of positive amino acids in the recognition site. Current mutational data has been focused on amino acid properties suggested to be critical for

substrate transport. Amino acids with high conservation have been studied previously, but further investigation is necessary to determine the function of amino acids potentially involved in substrate positioning. Our group has targeted many amino acids for mutational effect on the transport of thyroxine. Selection was based on amino acid location within the putative pore, conservation throughout the Oatps, and side chain volume effects on substrate recognition.

Alpha helix 2 has the highest conservation amongst the Oatps according to compiled data displayed in Fig. 6. High conservation across Oatps indicates evolutionary importance for structural integrity or substrate recognition. Conserved polar amino acid mutations created in Helix 2 (D85A, E89A, and N92A) were observed to display expression in perinuclear regions with no plasma membrane localization, and no uptake of ^{125}I-T_4 using HEK293 cells [21]. From these previous studies, it is possible that transmembrane domain 2 is important for proper Oatp1c1 folding, where irregularities in folding may increase cellular trapping and impede membrane localization. Unlike the mutations created by Westholm et al. (D85A, E89A and N92A), Oatp1c1 mutations F88L, F88A, I96A, and I96S in helix 2 show protein localization at the plasma membrane similar to wild type, with only slight intracellular trapping. From these previous studies, it is possible that transmembrane domain 2 is important for proper Oatp1c1 folding, where irregularities in folding may increase cellular trapping and impede membrane localization. Novel mutations to Helix 2 were designed to be more subtle, and included: F88L, F88A, I96A and I96S. These mutant constructs showed plasma membrane localization as seen in Fig. 11. F88L and I96S had thyroxine uptake equal to that of

empty vector. F88A and I96A displayed thyroxine uptake greater than empty vector but less than WT at approximately 75 and 67%, respectively (Fig. 9 and 10). To further characterize the importance of these mutations a full time course was carried out for determining the linear range of thyroxine uptake, and a 6 minute time point was chosen to study the effects of each mutation on protein kinetics (Fig. 13B). Time course data (Fig. 13B) is consistent with 10 minute screens (Fig. 9, 10 and 12), and displays a rapid influx of radiolabeled ^{125}I-T_4 initially. Upon kinetic profile evaluation, velocity is concentration dependent at concentrations of thyroxine less than 22 nM (Fig. 14B and 14C). As concentration increases above 22 nM, a leveling of velocity occurs that lacks the biphasic profile in both F88A and I96A stably transfected mutant constructs.

In mutant construct F88A the velocity leveling indicates that the high affinity binding site remained unaffected by the mutation, while the low affinity binding site was completely abolished (Fig. 15C). Closer inspection of the low concentration range (1-80 nM) resembled a standard Michaelis-Menten curve with a high affinity binding site K_m of 9 nM which was not statistically less than WT (Fig. 14C). Phenylalanine 88 may play a structural role for substrate access to both possible binding sites by using the side chain volume to interact with adjacent α-helices, pushing them in such a way that two binding sites are accessible. It is also possible that the two predicted binding sites may not overlap, but function simultaneously, which is why a loss of one binding site is observed. If the putative pore had a single channel, the truncation of a large nonpolar amino acid to alanine could reduce steric constraints and make the putative protein pore larger.

However, removal of the phenyl group appears to cause an α-helix interaction where the hypothetical low affinity binding site collapses.

Mutant construct F88L appeared to completely abolish 1 nM thyroxine uptake at room temperature and six minutes. Protein was less localized to the plasma membrane than WT, meaning the mutation may have affected the required folding and localization process (Fig. 11). Phenylalanine 88 appears to have importance in substrate recognition or structural integrity. By replacing the benzyl side chain on phenylalanine with an isobutyl group (leucine), effectively reducing the side chain volume, the affect on transport should be minimal but, as shown, it is quite significant. The phenylalanine side chain could be responsible for protein structural integrity and substrate positioning within the putative pore. A structural mutation might result in an α-helix orientation that constrains the primary substrate recognition site.

Mutant construct I96A (Fig. 4-8) displayed typical Michaelis-Menten kinetics consistent with a single saturable substrate site (Fig. 15B). Wild type Oatp1c1 is shown to have atypical, biphasic kinetics (Fig. 15A). Saturation of I96A occurred at approximately 25 nM, much lower than the 100nM concentration estimated for the high affinity binding saturation of WT Oatp1c1. The K_m for I96A was 12 nM, and for WT it was 16 nM. The mutation of Ile96 to alanine appears to have knocked out the low affinity binding site completely, removing the biphasic kinetic profile seen in WT Oatp1c1. Isoleucine is a nonpolar amino acid with an aliphatic side chain that may be involved in the recognition and transport of hydrophobic ligands. By changing Ile96 to alanine, the hydrophobic side

chain is truncated and the low affinity binding site function is abolished. It is possible that the side chain truncation caused a shift in surrounding transmembrane domains, leading to a pore size constriction. The K_m is also less than WT meaning that substrate binding might be stronger in I96A mutant constructs.

Transmembrane domain 5 is predicted to house 26 amino acids, making it longer than other transmembrane domains by up to 8 amino acids. Tyrosine 227 lies just on the intracellular side of alpha helix 5. Tyrosine 227 was converted to an alanine in one construct, and a leucine in another. Mutant construct Y227A had positive expression in HEK293 cells, with cytoplasmic staining, and punctate membrane localization. Thyroxine transport was greater than empty vector, but much less than WT. This change in thyroxine transport was considered a result of the inefficient plasma membrane localization and was not tested further. Y227L expression was highly localized to the plasma membrane and at 6 minutes, showed thyroxine transport slightly higher than WT. Further kinetics analysis was carried out and the Michaelis-Menten constant for Y227L was determined to be 8 nM, which is similar to WT. (Fig. 14D). From Fig. 14 it is evident that Y227L has a higher affinity for thyroxine and reaches equilibrium more rapidly. Tyrosine has a hydroxyl group that may be involved in hydrogen bonding for WT Oatp1c1. When converted to a leucine, the hydrogen bonding is lost and a truncation of the side chain could result in slight structural constriction. Because the location of amino acid 227 is bordering the intracellular plasma membrane, pore size constriction, by converting tyrosine to leucine at this location might result in a slight funnel shape which increases the amount of time thyroxine spends within the putative pore which may cause

the observed increase in affinity. Other than a speculation on why the increase in affinity, the only justified conclusion is that this mutation is not critical for function.

Phenylalanine 243, found in α helix 5 and thought to be adjacent to arginine 601 within the putative pore, was mutated to an alanine (F243A) for one construct and a leucine (F243L) for another. Uptake of 1 nM ^{125}I-T_4 at ten minutes in transiently transfected HEK293 cells showed total protein transport equal to empty vector in F243A (Fig. 10). This came as a surprise because F243A expression was highly localized to the plasma membrane (Fig. 11). The phenyl group of Phe243 might play a key role in positioning anionic substrates for recognition by conserved Arg601. By converting Phe243 to alanine, the phenyl group is removed and the steric constraint for localization is relaxed. Expression of F243L was not localized to the plasma membrane and therefore was not studied further. Transmembrane domain 5 mutagenesis has not been performed in any other studies.

Transmembrane domain 7 has relatively low conservation amongst the Oatps. Phenylalanines 370 and 374 reside in transmembrane domain 7, and both were targeted for site directed mutagenesis to alanine and leucine. Initial screening of F370A displayed T_4 uptake to be less than WT and greater than Empty vector (Fig. 9). Expression of F370A displayed localization predominantly to the plasma membrane (Fig. 11). A full time course was completed using 1nM ^{125}I-T_4 from 0 to 60 minutes (Fig. 13E) for F370A and displayed uptake (fmol/mg protein) greater than WT, possibly from a higher protein concentration. Evaluation of kinetics showed K_m values for F370A similar to WT.

Transmembrane domain 7 is interchangeable in OATP1B1 and OATP1B3 without impacting the transport of estradiol-17β-D-glucuronide which agrees with the limited impact of Phe370 mutation on Oatp1c1 transport [62]. The lack of effect in both cases suggests helix 7 has little influence on the Oatp recognition site. Phenylalanine 374 is also located in α-helix seven. Initial uptake screening and full time course measurement showed T_4 uptake by F374A was greater than empty vector and less than WT (Fig. 9). Based on immunohistochemistry staining of transiently transfected HEK293 cells, F374A showed punctate staining at the plasma membrane consistent with reduced uptake. The Michaelis constant was determined to be 25 nM compared to 16 nM displayed in WT (Fig. 14F).

Performing site directed mutagenesis to the transporter Oatp1c1 has resulted in gained insight into protein structure and some of the important characteristics associated with thyroxine recognition. We have further confirmed the structure hypothesized by Westholm et al [21] as having strong predictive value. Mutations successfully determined amino acids involved in thyroxine transport and recognition as well as residues important for Oatp1c1 structural integrity.

Overall, these results might indicate the presence of non-overlapping high affinity and low affinity binding sites. This was demonstrated by the apparent biphasic profile associated with WT, as well as the characterization of I96A using the mutations created in our laboratory. Based on results from alpha helix 2 mutations, future tests should be performed using the Oatp1c1 substrate, $E_2$17βG. It is previously known that $E_2$17βG

displays biphasic kinetics but recognizes Oatp1c1 binding sites differently than T_4 [53]. Alpha helix 2 importance in substrate recognition can be determined by K_m examination using $E_2$17βG as a substrate against alpha helix 2 mutant constructs: F88A, F88L, I96A, and I96S. If the K_m changes for $E_2$17βG in the same manner as T_4, alpha helix 2 can be considered important. The change in substrate to $E_2$17βG using the same mutant constructs will give us further insight into amino acids important for transport. With combined knowledge of amino acids essential for substrate recognition and transport, novel drugs can be created for successful transport across the blood brain barrier by Oatp1c1-dependent transport mechanisms.

Tables

Mutation	Primer Sequence
F88A	5'-301-ctggtgggaataattgatggtagtGCAgaaattgggaatctcctggtcata-3'
F88L	5'-301-ctggtgggaataattgatggAagCttGgaaattgggaatctcctggt-3'
I96A	5'-326-cgaaattgggaatctcctggtcGCGacattcgttagctactttggtg-3'
I96S	5'-328-aaattgggaatctcctggtcaGTacTttcgttagctactttggtgcc-3'
Y227A	5'-662-gtgaagacaatgctgccttcGCAatcgggtgtgtgcagacagt-3'
Y227L	5'-664-gaagacaatgctgccttcCTGatcgggtgtgtgcagac-3'
F243A	5'-709-attatagggcccattttcggcGCGctcttgggttcattatgtgcc-3'
F243L	5'-711-tatagggcccattttcggcCtcctACtgggttcattatgtgccaa-3'
F370A	5'-1089-ttgtgtgcaagcactgttcagGCGaattctctattcggcatggtc-3'
F370L	5'-1091-gtgtgcaagcactgttcagCtGaattctctattcggcatgg-3'
F374A	5'-1092-tgtgcaagcactgttcagttcaattctctGGCcggcatggtcacata-3'
F374L	5'-1096-caagcactgttcagttcaattctctaCTGggcatggtGacatataaaccaaagtac-3'

Table 1 Primers were designed to create point mutations of wild type plasmid DNA. Forward primers are shown above and reverse complement primers were also used for mutagenesis. Mutation is in the format XnZ, where X is the WT amino acid, n is the amino acid number within Oatp1c1, and Z is the new amino acid following mutagenesis. Capitalized letters in primer sequences represent nucleotides changed from WT Oatp1c1 to form the mutation and the underlined section is the novel restriction site. Primer sequences are from 5' to 3' with corresponding nucleotide number, within the Oatp1c1 gene, labeled at the beginning.

FIGURES

A.

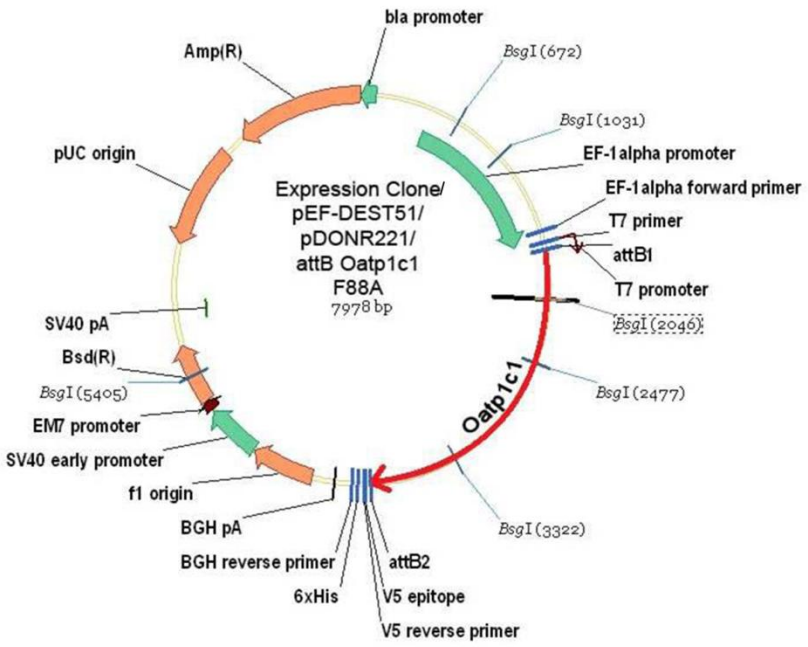
bla promoter
Amp(R)
BsgI (672)
BsgI (1031)
pUC origin
EF-1 alpha promoter
EF-1 alpha forward primer
Expression Clone/
pEF-DEST51/
pDONR221/
attB Oatp1c1
F88A
7978 bp
T7 primer
attB1
T7 promoter
BsgI (2046)
SV40 pA
Bsd(R)
BsgI (5405)
Oatp1c1
BsgI (2477)
EM7 promoter
SV40 early promoter
f1 origin
BGH pA
BsgI (3322)
BGH reverse primer
attB2
6xHis
V5 epitope
V5 reverse primer

B.

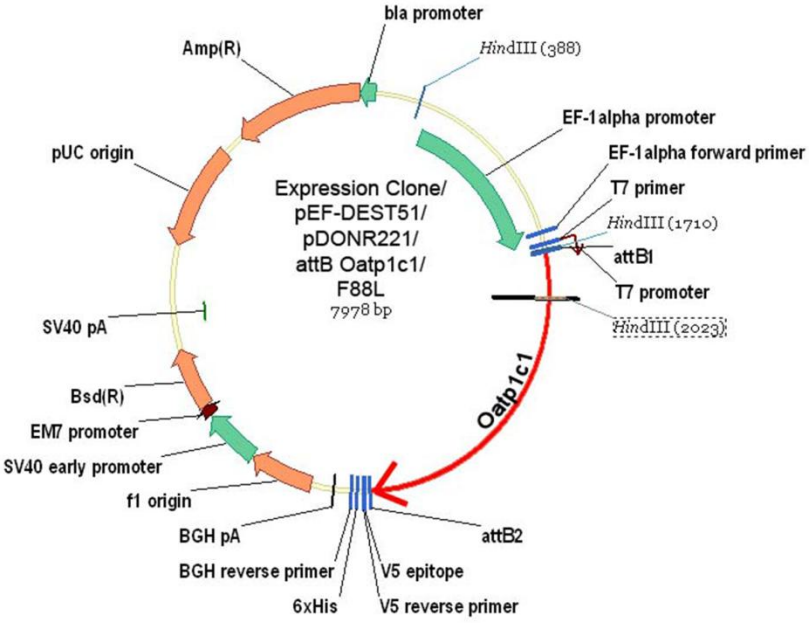
bla promoter
Amp(R)
HindIII (388)
EF-1 alpha promoter
pUC origin
EF-1 alpha forward primer
Expression Clone/
pEF-DEST51/
pDONR221/
attB Oatp1c1/
F88L
7978 bp
T7 primer
HindIII (1710)
attB1
T7 promoter
HindIII (2023)
SV40 pA
Bsd(R)
Oatp1c1
EM7 promoter
SV40 early promoter
f1 origin
BGH pA
attB2
BGH reverse primer
V5 epitope
6xHis
V5 reverse primer

C.

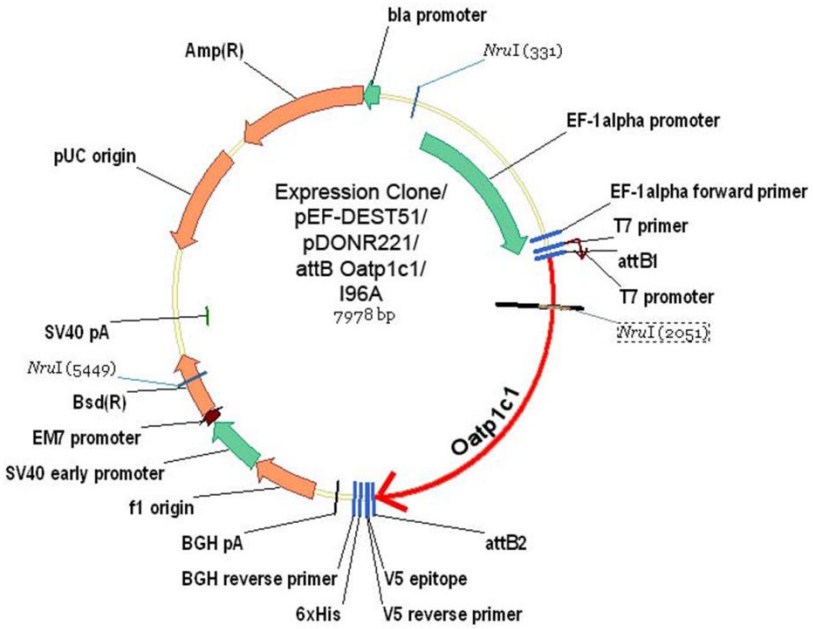
bla promoter
Amp(R)
NruI (331)
EF-1 alpha promoter
pUC origin
Expression Clone/
pEF-DEST51/
pDONR221/
attB Oatp1c1/
I96A
7978 bp
EF-1 alpha forward primer
T7 primer
attB1
T7 promoter
NruI (2051)
SV40 pA
NruI (5449)
Bsd(R)
EM7 promoter
SV40 early promoter
f1 origin
Oatp1c1
BGH pA
attB2
BGH reverse primer
V5 epitope
6xHis
V5 reverse primer

D.

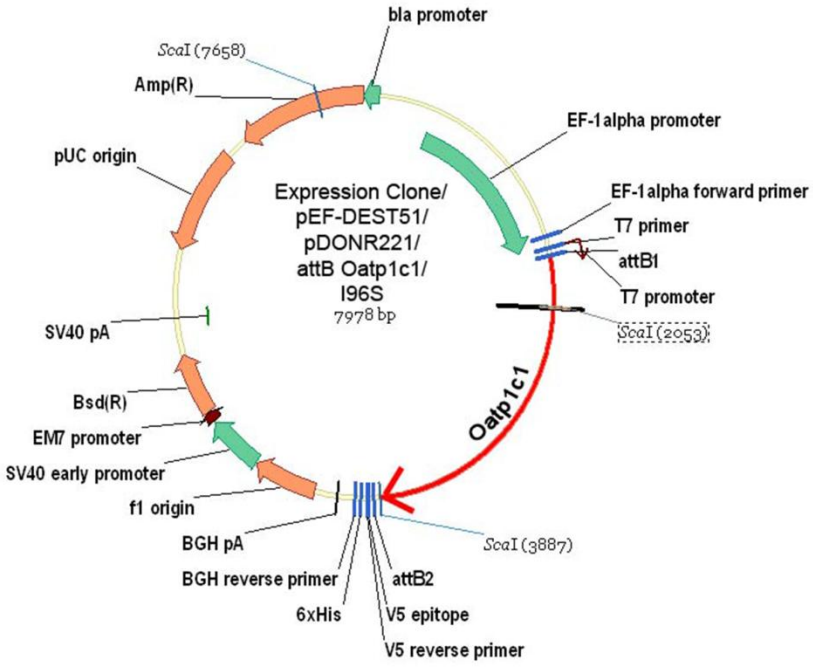
bla promoter
ScaI (7658)
Amp(R)
EF-1 alpha promoter
pUC origin
Expression Clone/
pEF-DEST51/
pDONR221/
attB Oatp1c1/
I96S
7978 bp
EF-1 alpha forward primer
T7 primer
attB1
T7 promoter
ScaI (2053)
SV40 pA
Bsd(R)
EM7 promoter
SV40 early promoter
f1 origin
Oatp1c1
BGH pA
ScaI (3887)
BGH reverse primer
attB2
6xHis
V5 epitope
V5 reverse primer

E.

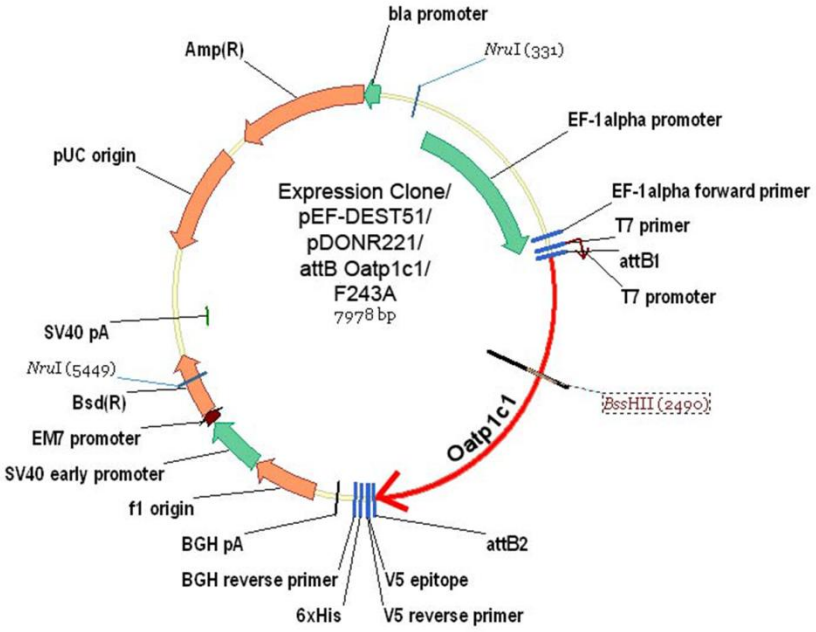
bla promoter
Amp(R)
NruI (331)
EF-1 alpha promoter
pUC origin
Expression Clone/
pEF-DEST51/
pDONR221/
attB Oatp1c1/
F243A
7978 bp
EF-1 alpha forward primer
T7 primer
attB1
T7 promoter
SV40 pA
NruI (5449)
Bsd(R)
EM7 promoter
SV40 early promoter
f1 origin
BGH pA
BGH reverse primer
6xHis
V5 epitope
V5 reverse primer
attB2
Oatp1c1
BssHII (2490)

F.

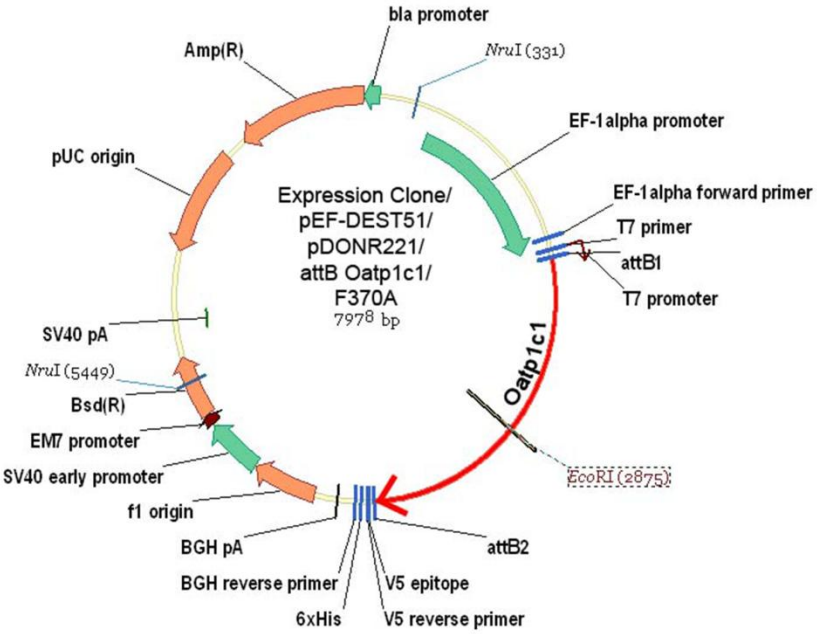
bla promoter
Amp(R)
NruI (331)
EF-1 alpha promoter
pUC origin
Expression Clone/
pEF-DEST51/
pDONR221/
attB Oatp1c1/
F370A
7978 bp
EF-1 alpha forward primer
T7 primer
attB1
T7 promoter
SV40 pA
NruI (5449)
Bsd(R)
EM7 promoter
SV40 early promoter
f1 origin
BGH pA
BGH reverse primer
6xHis
V5 epitope
V5 reverse primer
attB2
Oatp1c1
EcoRI (2875)

G.

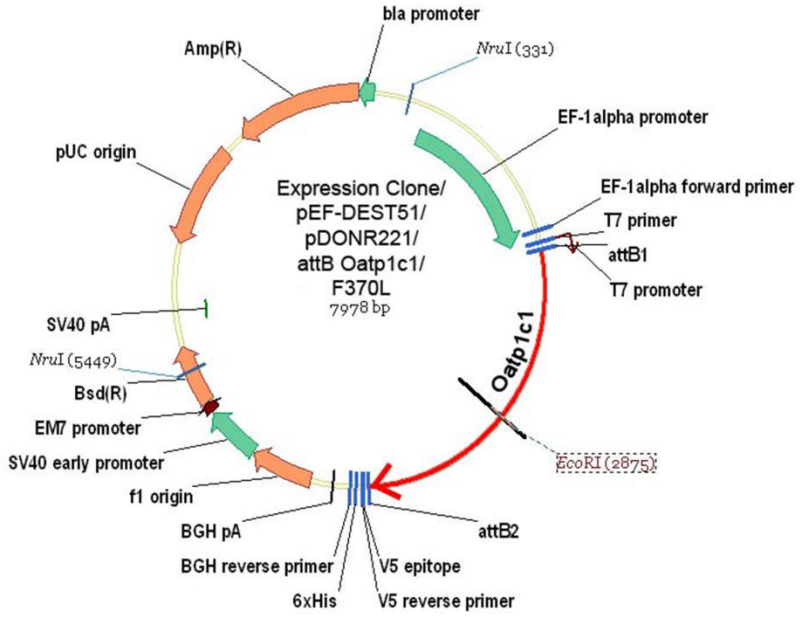
bla promoter
Amp(R)
NruI(331)
EF-1alpha promoter
pUC origin
Expression Clone/
pEF-DEST51/
pDONR221/
attB Oatp1c1/
F370L
7978 bp
EF-1alpha forward primer
T7 primer
attB1
T7 promoter
Oatp1c1
SV40 pA
NruI(5449)
Bsd(R)
EM7 promoter
SV40 early promoter
EcoRI(2875)
f1 origin
BGH pA
attB2
BGH reverse primer
V5 epitope
6xHis
V5 reverse primer

H.

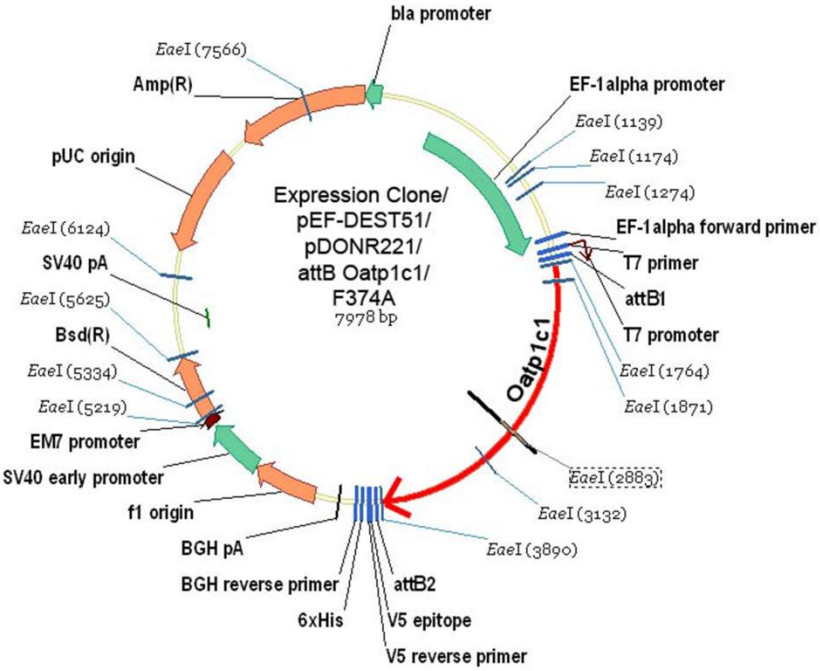
bla promoter
EaeI(7566)
Amp(R)
EF-1alpha promoter
EaeI(1139)
EaeI(1174)
pUC origin
EaeI(1274)
Expression Clone/
pEF-DEST51/
pDONR221/
attB Oatp1c1/
F374A
7978 bp
EF-1alpha forward primer
EaeI(6124)
T7 primer
SV40 pA
attB1
EaeI(5625)
T7 promoter
Bsd(R)
EaeI(1764)
EaeI(5334)
EaeI(1871)
EaeI(5219)
Oatp1c1
EM7 promoter
EaeI(2883)
SV40 early promoter
EaeI(3132)
f1 origin
EaeI(3890)
BGH pA
BGH reverse primer
attB2
6xHis
V5 epitope
V5 reverse primer

I.

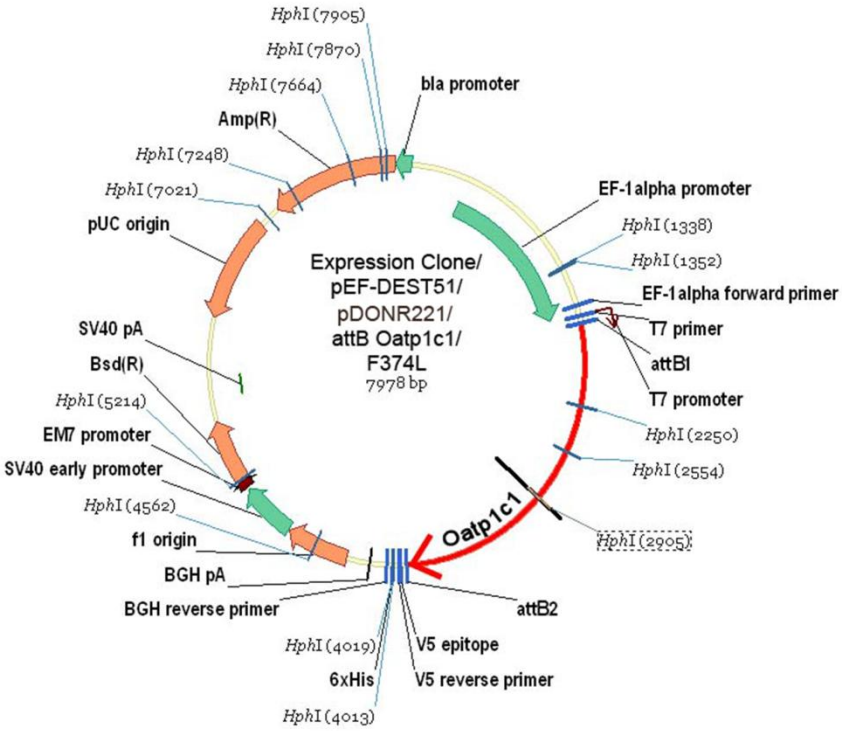

Figure 1 Restriction digest maps of Oatp1c1 mutants expressed in pEF-DEST51 expression vector. Bold, black lines, on the red Oatp1c1 gene insert, indicate where the mutation and cryptic cut site occurred (also depicted by dashed box surrounding restriction enzyme name). Numbers, next to the restriction enzyme site, represent the nucleotide restriction site location. Novel restriction sites use varying restriction enzymes: A. F88A cut with BsgI B. F88L cut with HindIII C. I96A cut with NruI D. I96S cut with ScaI E. F243A cut with BssHII and NruI F. F370A cut with EcoRI and NruI G. F370A cut with EcoRI and NruI H. F374A cut with EaeI H. F374L cut with HphI.

BsgI	
F88A	WT
3245	3245
2083	2083
1015	1446
845	845
431	359
359	

HindIII	
F88L	WT
6343	6606
1322	1322
313	

NruI	
I96A	WT
3398	5118
2860	2860
1720	

ScaI	
I96S	WT
3771	4207
2373	3771
1834	

NruI and BssHII	
F243A	WT
2955	5118
2860	2860
2163	

NruI and EcoRI	
F370A/L	WT
2860	5118
2574	2860
2544	

EaeI	
F374A	WT
1016	1261
758	758
245	107
107	22
22	
2	

HphI	
F374L	WT
1025	1358
488	488
333	304
304	

Figure 2 Restriction enzymes (top) were used to verify cryptic cut site formation. Using each restriction enzyme, mutation containing plasmid DNA (left column) could be distinguished from WT DNA (right column) by fragment quantity and size (base pairs) when run on an agarose gel.

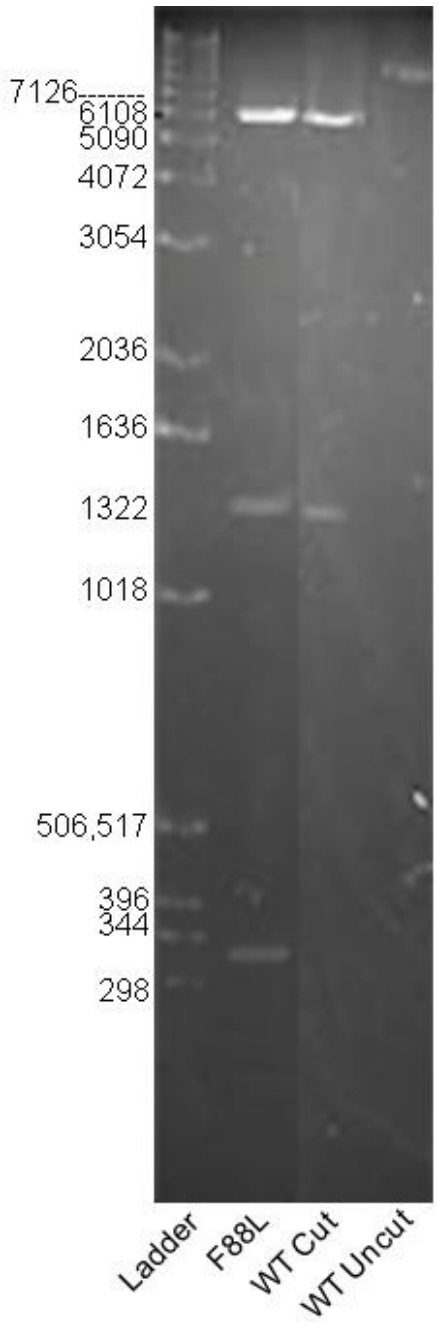

Figure 3 Example of restriction digest for determination of cryptic cut site insertion. One microgram of WT and mutant construct F88L DNA was digested with HindIII for one hour at 37^0 C. DNA was run on a 1% Seakem agarose gel for two hours at 90 V. Three microliters of kaleidoscope ladder were run in the left lane (Ladder). Fragment sizes found for mutant construct F88L indicate that a restriction site has been inserted with expected banding pattern (6343, 1322, and 313 base pairs) from Fig. 2. WT DNA was subjected to HindIII digestion and obtained the banding pattern expected (6606 and 1322 base pairs). WT uncut DNA was run as a plasmid without exposure to HindIII.

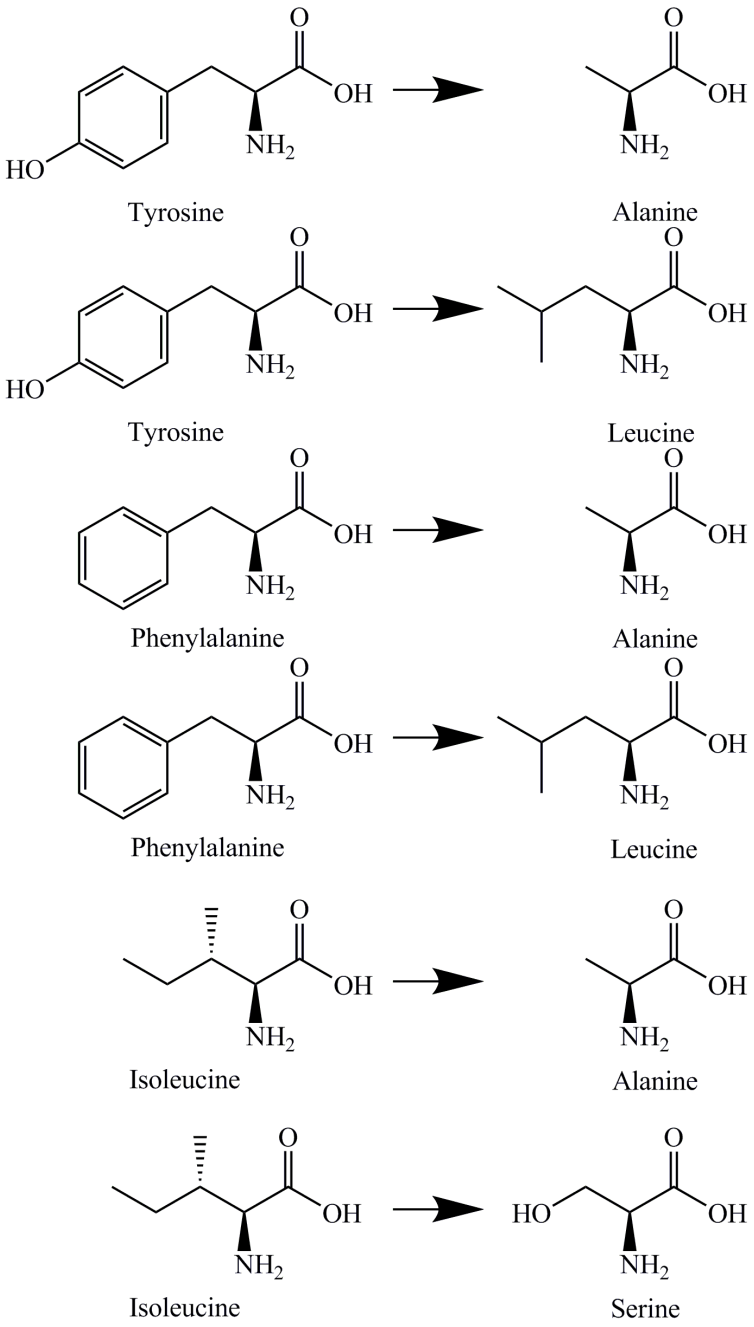

Figure 4 Amino acids on the left are the targeted amino acids for mutation, while the amino acids on the right indicate the new amino acid and structure following mutation. Site-directed mutagenesis of tyrosine to alanine or leucine truncates the side chain length and removes the aromatic ring as well as the hydroxyl group involved in hydrogen bonding. When phenylalanine is mutated to alanine or leucine, the aromatic ring is removed, and the side chain shortened, allowing freedom from steric constraints imposed on substrate transport. Isoleucine was mutated to alanine for side chain truncation and to serine for inclusion of an uncharged polar side chain. Alanine and leucine were chosen for amino acid replacement due to α-helix stabilization.

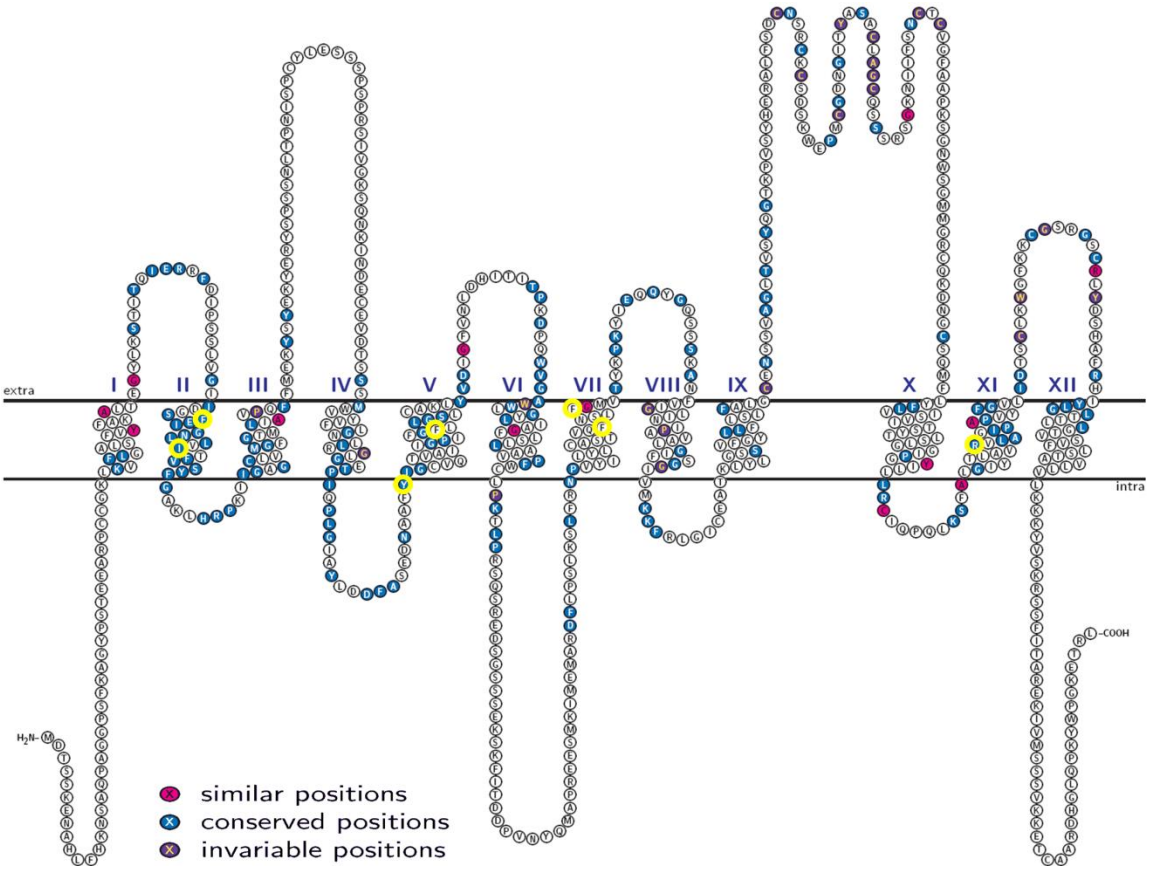

Figure 5 Amino acid sequence of Oatp1c1 with predicted 12 trans-membrane spanning alpha helices topology where both the N- and C-terminus lie on the intracellular side. Oatp1c1 is 716 amino acids long and numbered starting at the N-terminus. Each circle represents an amino acid denoted by its one letter code. Colored amino acids are as follows: Purple- 100% conservation amongst Oatps, Blue- greater than 80% conservation amongst Oatps, Red- conservative amino acid changes, Yellow circle- represents targeted amino acids for mutagenesis. Helix 2 contains F88A/L and I96A/S, helix 5 contains Y227A/L and F243A/L, helix 7 contains F370A/L, and F374A/L, and helix 11 contains the R601 residue.

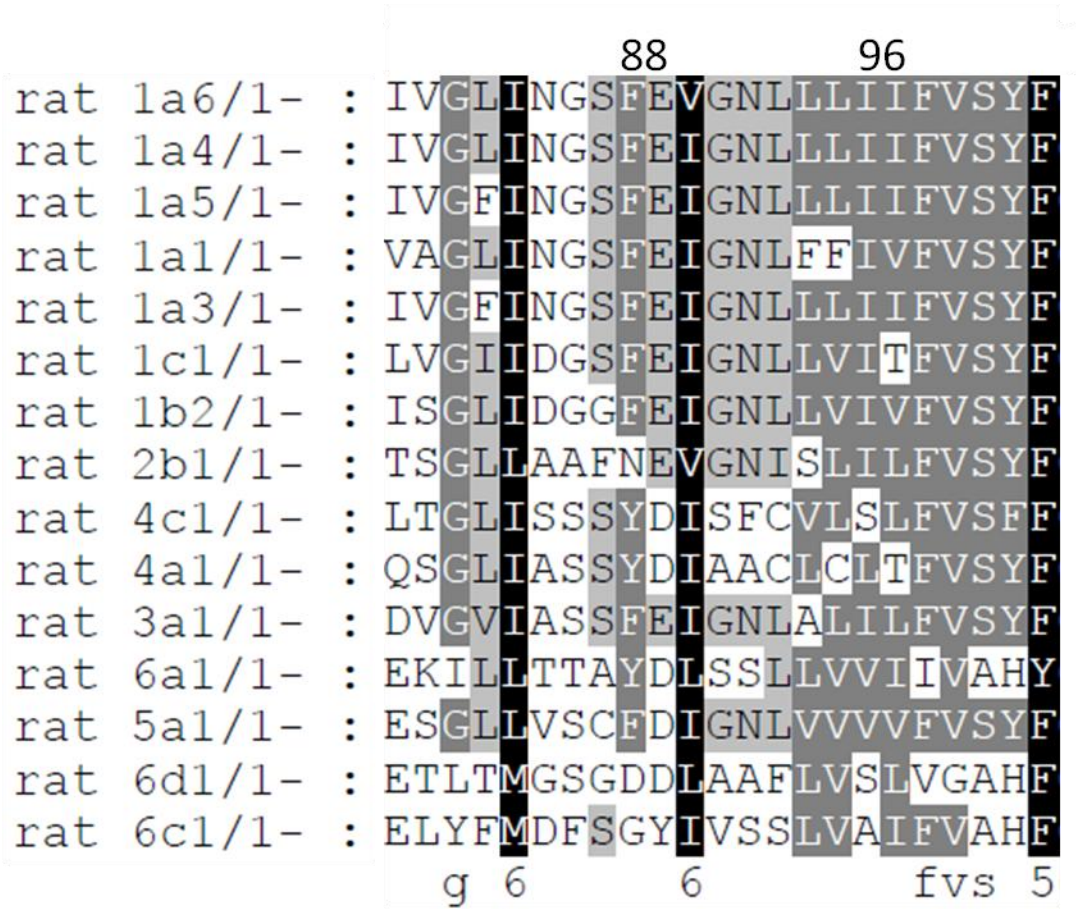

Figure 6 Oatp polypeptide sequence comparison for rats. Protein sequences of rat Oatps were determined using BLAST (NCBI) against rat Oatp1c1 and aligned using PROMALS. The darkness of background indicates the amount of homology from light gray, to gray to black, with black having the highest homology. Numbers above indicate the observed amino acids based on position within the Oatp1c1 polypeptide. Bottom numbers indicate homology level from 1-10, with 10 being the most homologous. Bottom letters indicate the highest conserved amino acid amongst the Oatps when non-similar amino acids are found within some Oatp sequences. Amino acids phe88 and ile96 were targeted for mutagenesis based on proximity of the conserved arg601 in the putative pore.

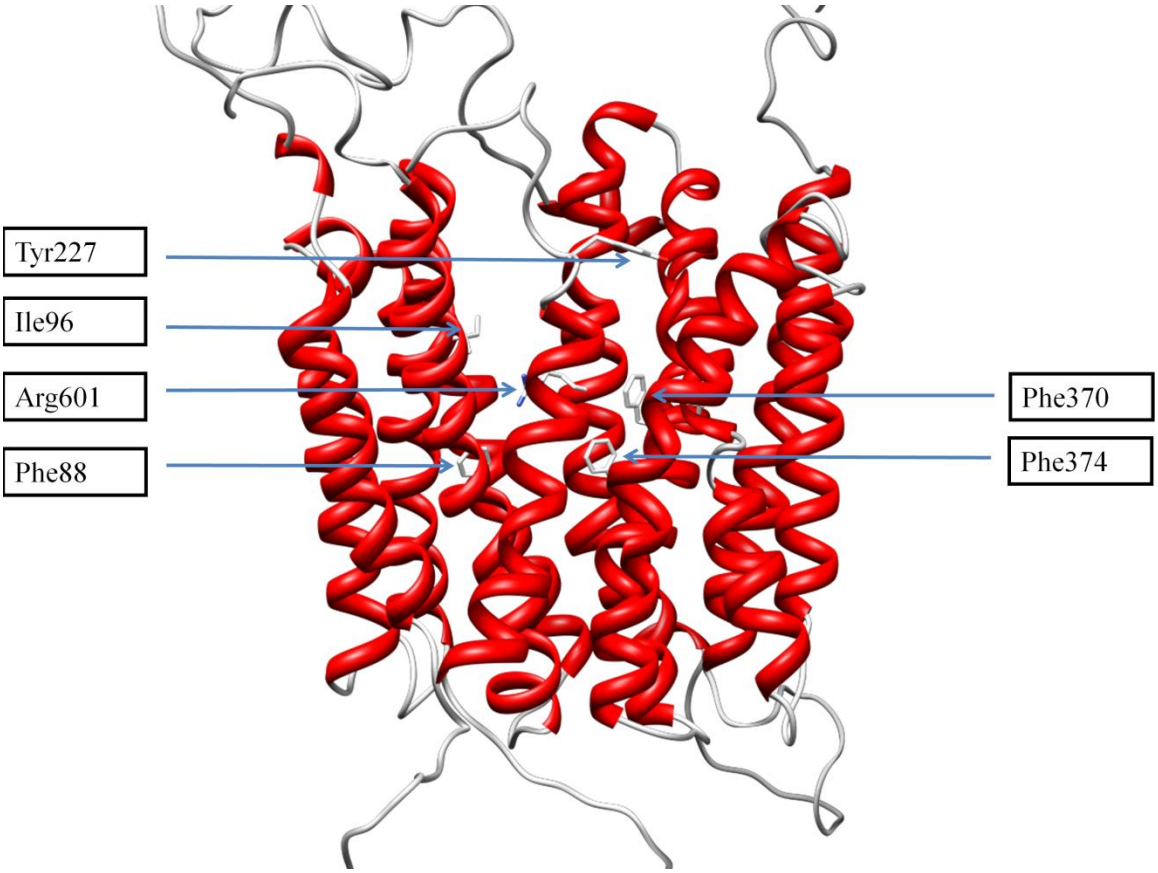

Figure 7 A predicted 3-D structure of Oatp1c1 based on the glycerol-3-phosphate crystal structure with amino acids targeted for mutation facing the central, putative pore. Red regions indicate transmembrane spanning α-helices. Amino acids shown have the side chain of the wild type amino acid and not the mutation. Arginine 601 plays a crucial role in structural modeling due to the conservation (>80%) amongst Oatps, the centrally located position within the glycerol-3-phosphate crystal structure, and the positively charged side chain which allows for the recognition of anionic substrates.

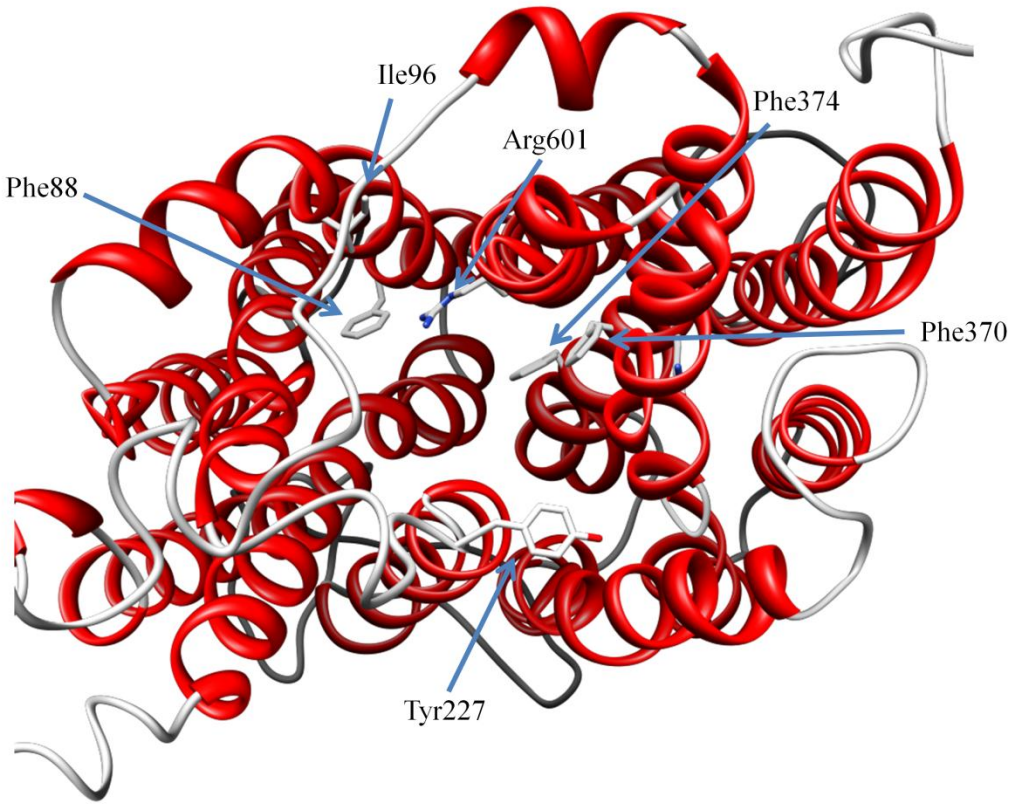

Figure 8 Top down view of 3-D Oatp1c1 model displaying amino acids targeted for mutation. The model indicates a central putative pore with amino acid side chains facing inward displaying possible steric constraints. Arginine 601 in alpha helix 11 is used as a reference point for hypothesized model.

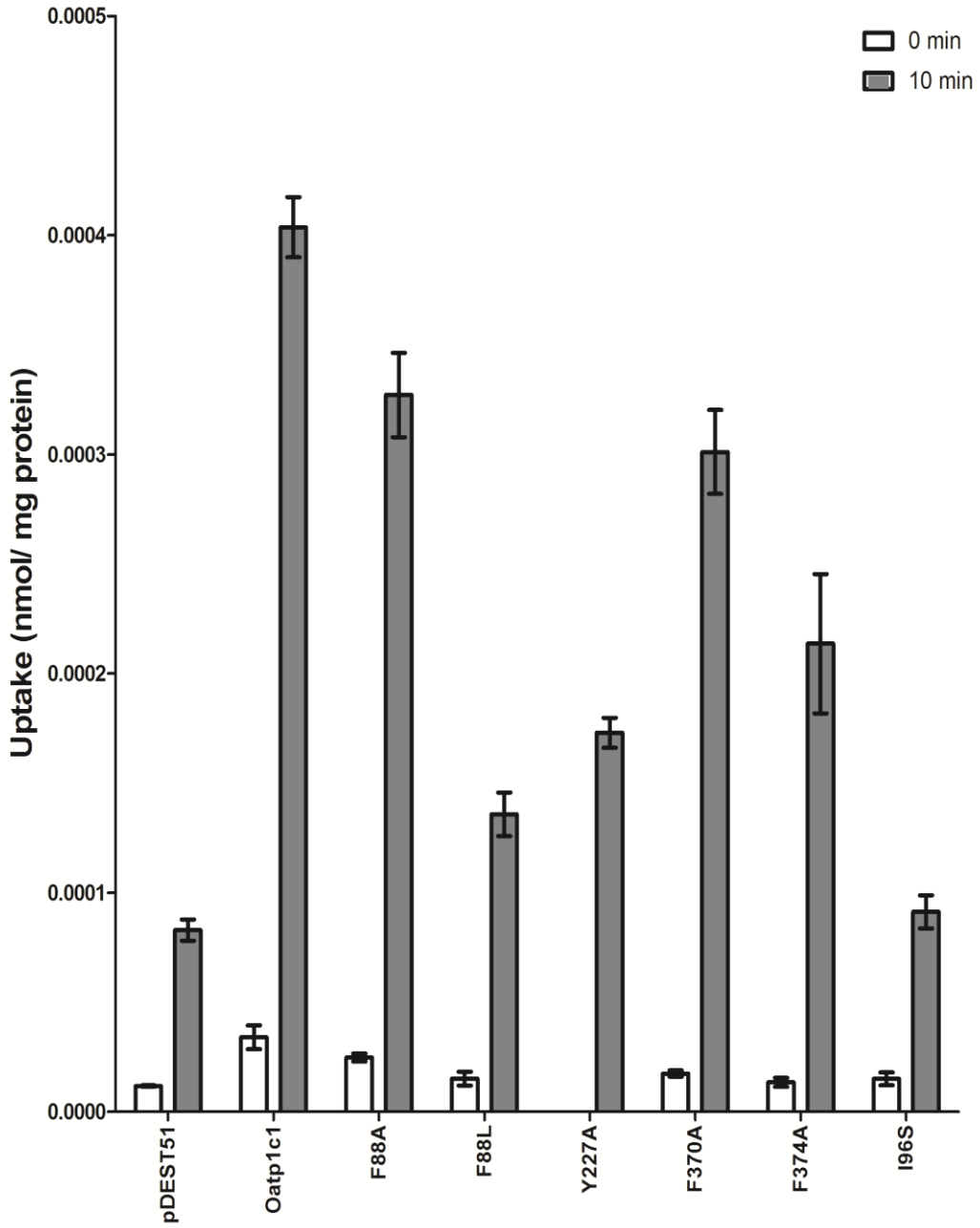

Figure 9 One nanomolar ^{125}I-T_4 uptake of transiently transfected Oatp1c1 versus empty vector at 0 and 10 minutes shown in nmol/mg total protein. A ten minute time point was used to screen ^{125}I-T_4 uptake by transiently transfected Oatp1c1. At ten minutes; WT Oatp1c1 had greater T_4 uptake than the empty vector counterpart. F88A, F88L, Y227A, F370A and F374A had greater uptake than empty vector at ten minutes, while uptake at zero minutes was essentially the same. I96S displayed T_4 uptake equal to empty vector at zero and ten minutes. Data represents mean±SEM of three replicate values.

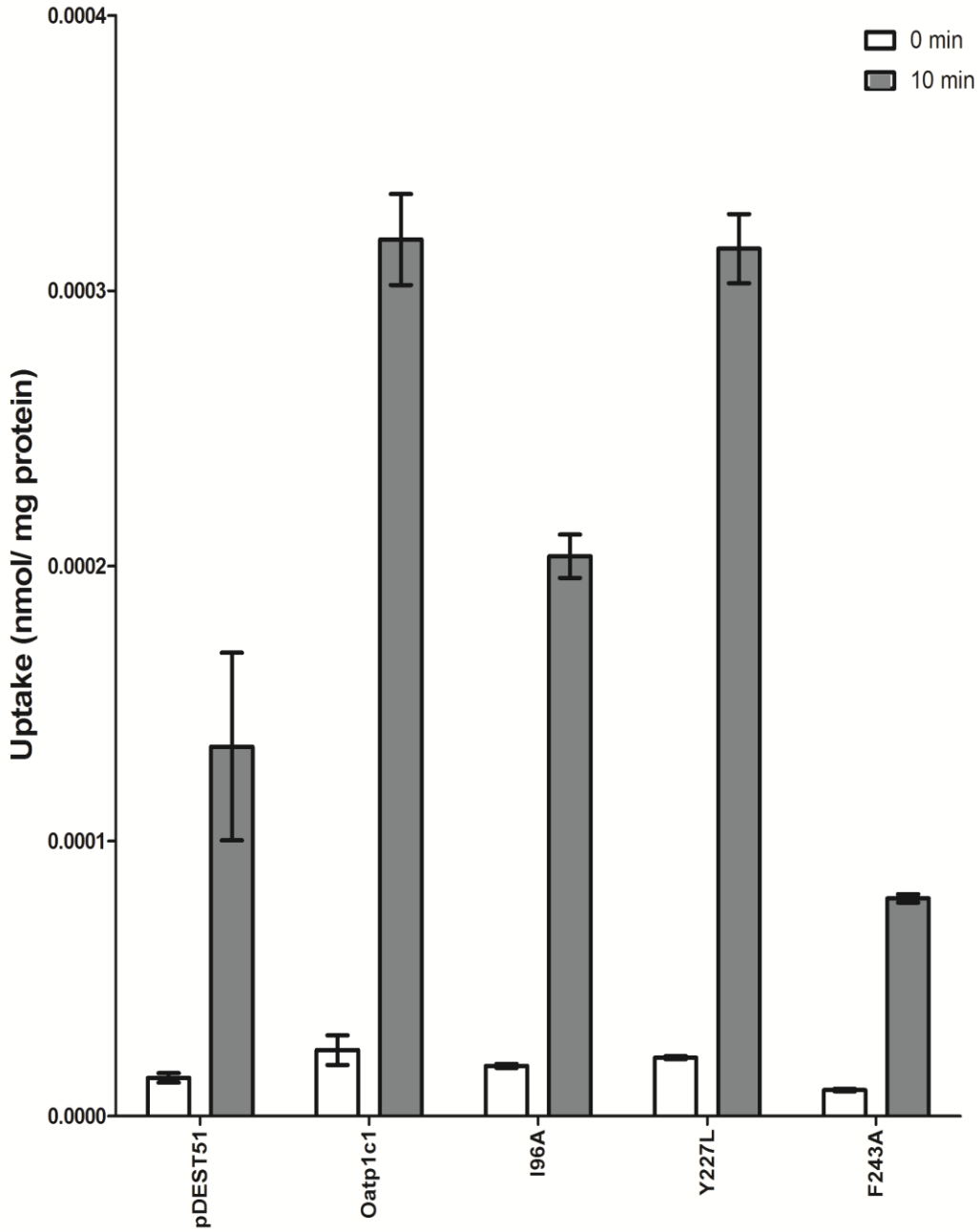

Figure 10 One nanomolar ^{125}I-T_4 uptake of transiently transfected Oatp1c1 versus empty vector at 0 and 10 minutes shown in nmol/mg total protein. Wild type Oatp1c1, I96A and Y227L had greater uptake than empty vector at ten minutes, while F243A had the same uptake as empty. Zero minute time points displayed similar uptake for all constructs. Data represents mean±SEM of three replicate values.

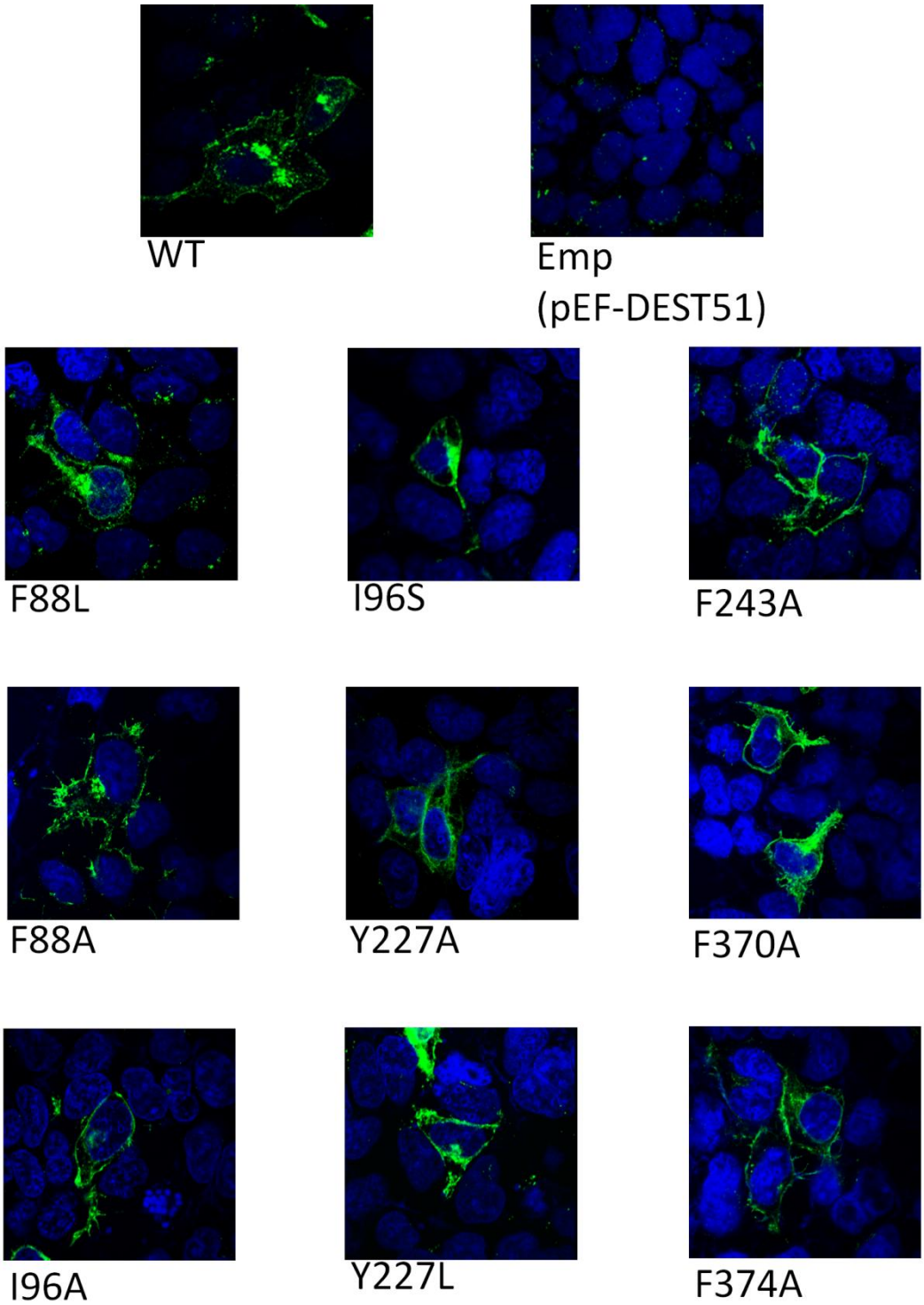

Figure 6 Immunohistochemistry staining of transiently transfected Oatp1c1 and mutants. Primary antibody is mouse anti-V5 antibody (Invitrogen, Carlsbad, CA), secondary antibody is goat anti mouse-FITC (Invitrogen, Carlsbad, CA) to show plasma membrane localization (in green) and the nuclei are stained with 4',6-diamidino-2-phenylindole (DAPI) (in blue). All pictures, save Empty vector, display plasma membrane localization.

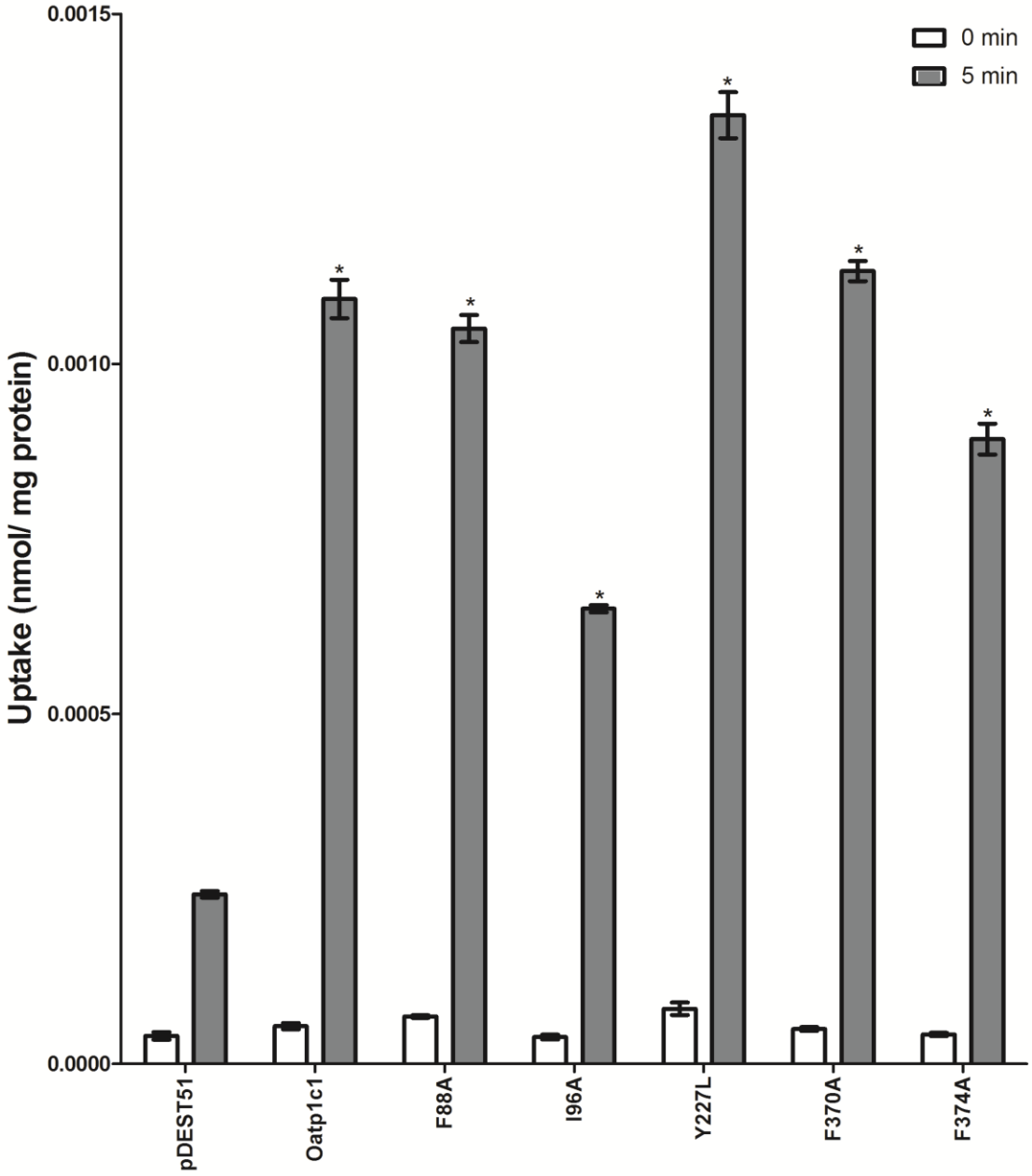

Figure 7 Uptake (nmol/mg total protein) of 1nm ^{125}I-T_4 by stably transfected Oatp1c1 and mutated Oatp1c1 at 0 and five minute time points show uptake greater than empty vector with Y227L greater than WT. Stably transfected Oatp1c1 and mutant counterparts were screened for ^{125}I-T_4 uptake at zero and five minutes. Uptake values are presented as mean±SEM of three replicate values. Two-way ANOVA with Bonferroni post test evaluated five minute time points of mutant constructs versus Empty vector using GraphPad Prism 5.02 for Windows, GraphPad Software, San Diego California USA). *$p < 0.001$

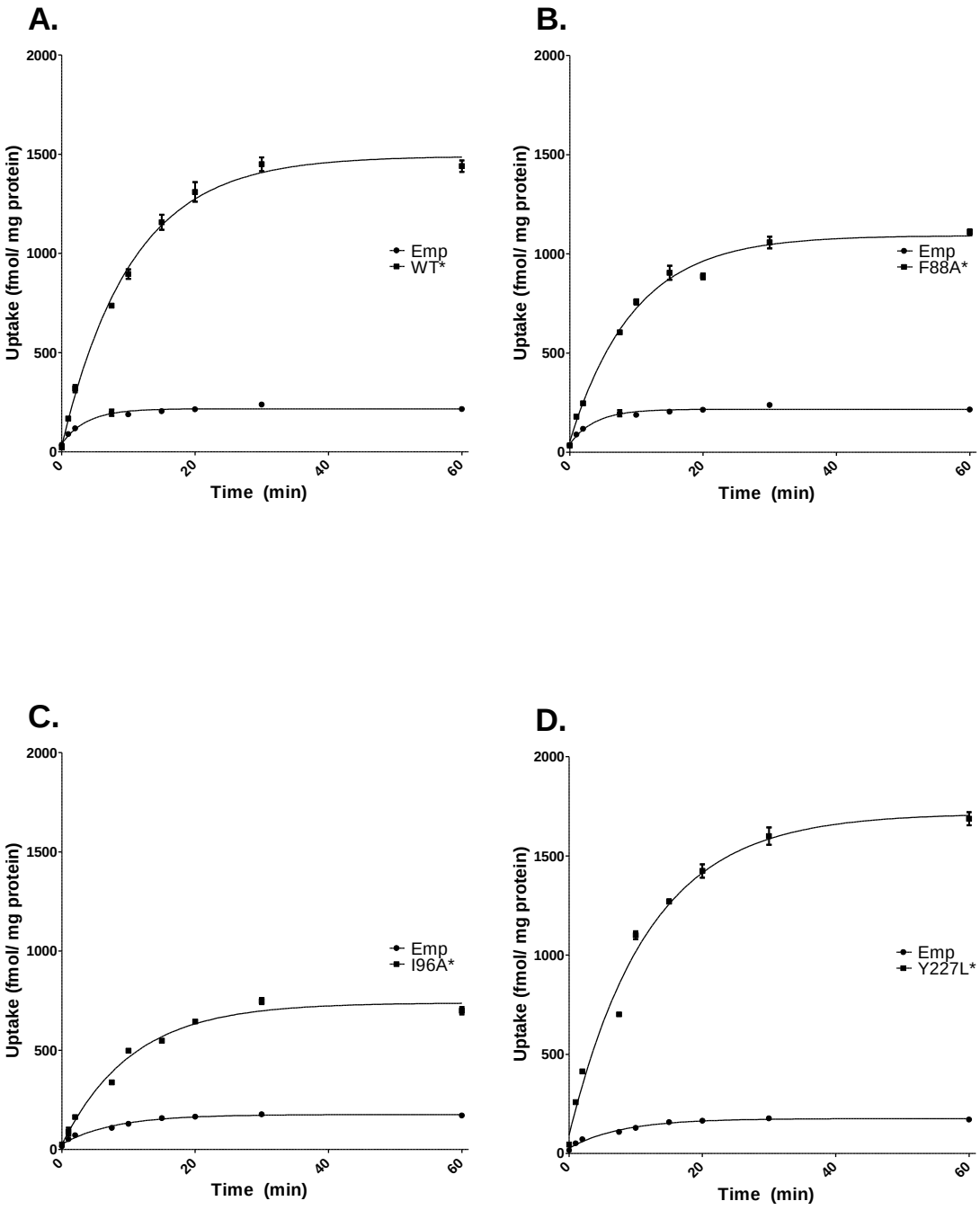
A.
B.
C.
D.
Uptake (fmol/ mg protein)
Time (min)
Emp
WT*
F88A*
I96A*
Y227L*
0
500
1000
1500
2000
20
40
60

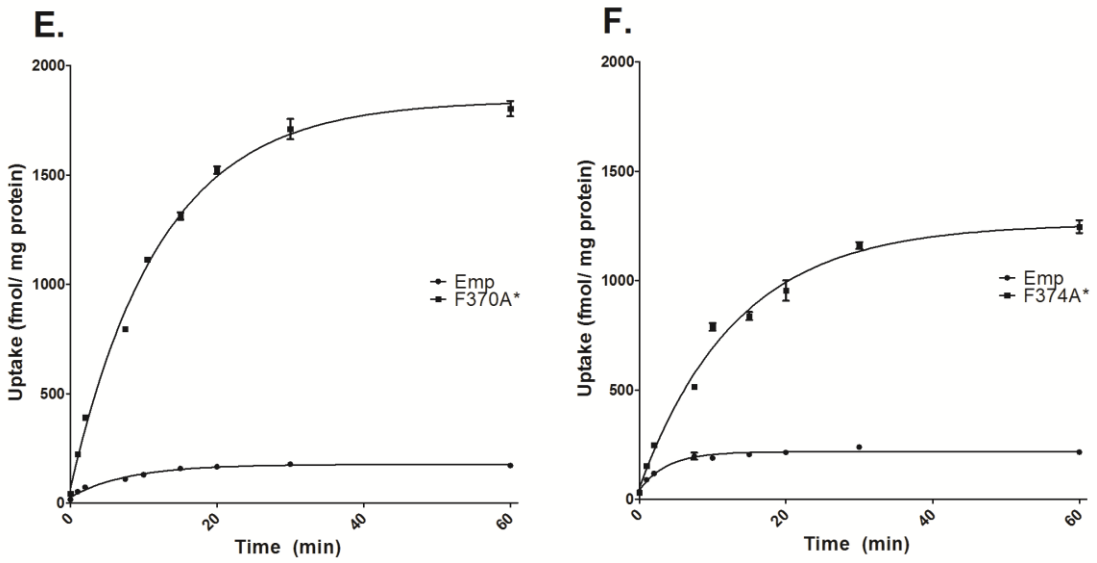

Figure 8 Time course uptake data of HEK293 cells stably transfected with Oatp1c1 mutants or empty vector. All mutants (A-F) have greater uptake than empty vector compared by two-way Anova with Bonferroni post-tests using GraphPad Prism 5.02 for Windows, GraphPad Software, San Diego California USA) to compare replicates, * is $P<0.0001$. Each data point is the mean ± SEM of three replicate trials.

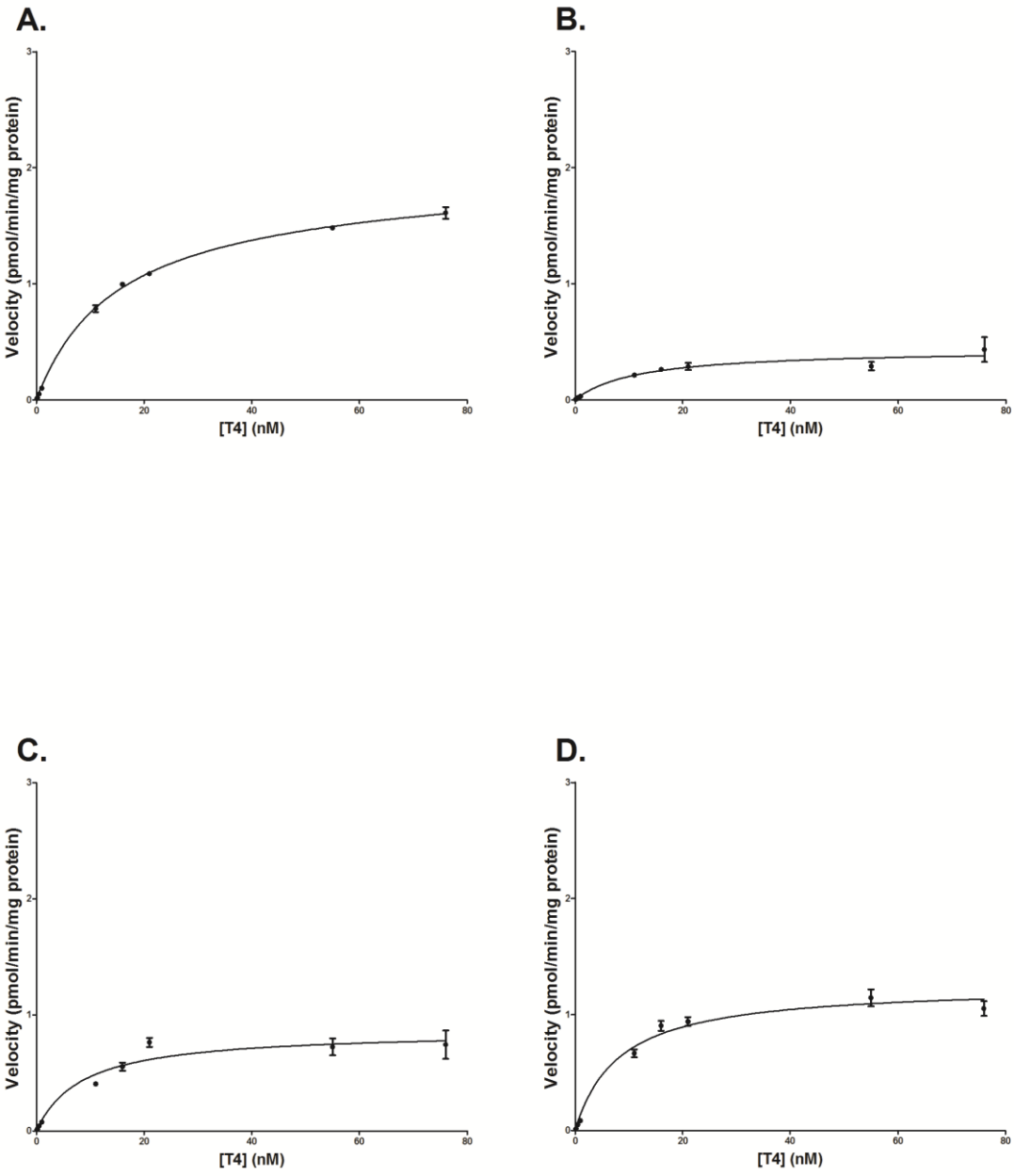
A.
B.
C.
D.
Velocity (pmol/min/mg protein)
[T4] (nM)
0
1
2
3
0
20
40
60
80

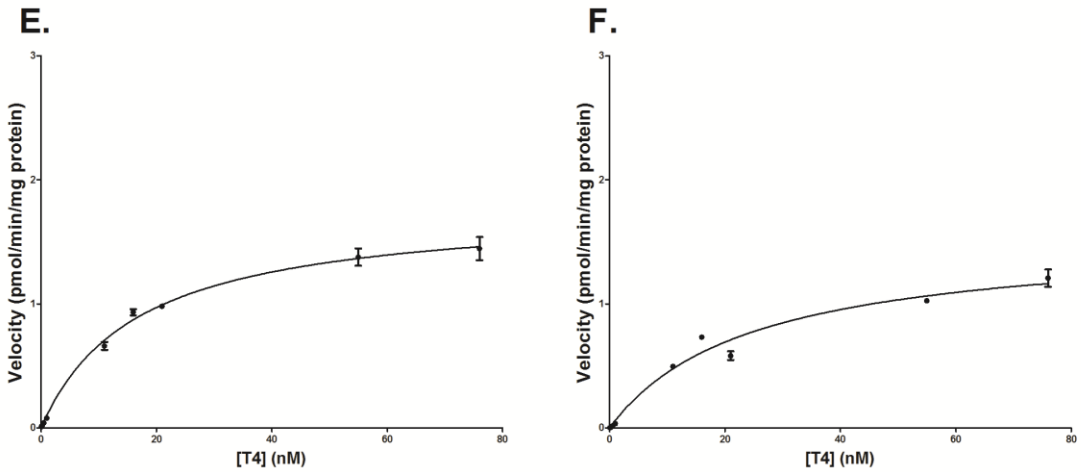

Figure 14 Michaelis-Menten kinetic assays on stably transfected HEK293 cells. Uptake of ^{125}I-T_4 was measured in pmol/ min/ mg total protein based on a six minute time-point. Data points represent the mean±SEM of three replicate trials and were fit to Michaelis-Menten kinetics using GraphPad Prism 5.02 for Windows, GraphPad Software, (San Diego, California USA) to determine K_m using a truncation of the complete concentration range A. WT (K_m = 16, R^2 = 0.99) B. I96A (K_m = 12, R^2 = 0.85) C. F88A (K_m = 9, R^2 = 0.92) D. Y227L (K_m = 8, R^2 = 0.97) E. F370A (K_m = 17, R^2 = 0.99) F. F374A (K_m = 25, R^2 = 0.97)

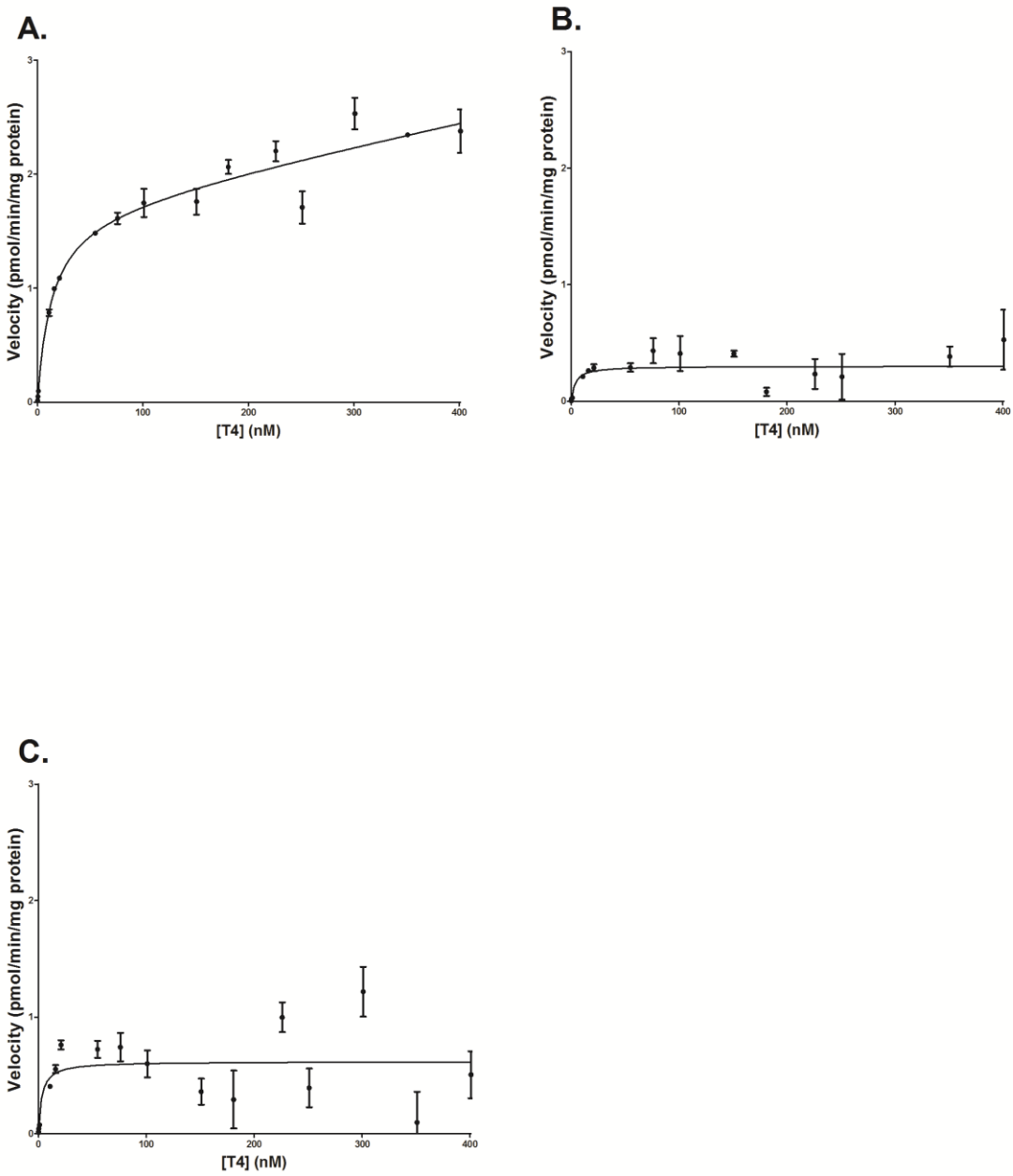

Figure 15 Alpha Helix 2 mutations eliminate biphasic kinetics. Full kinetic profiles of stably transfected HEK293 cells with **A.** WT displaying atypical, biphasic kinetics **B.** I96A showing one-site regular Michaelis Menten kinetics and **C.** F88A depicting one-site binding kinetics. Uptake of ^{125}I-T_4 was measured for varying concentrations at 6 minutes. At concentrations above 200 nM, a second, low affinity binding site appears to contribute to T_4 uptake in WT preventing a distinct V_{max} determination. Mutants I96A and F88A display Michaelis-Menten kinetics and lack the appearance of a second binding site. Points above 100 nM T_4 were not used for K_m determination in I96A nor F88A due to non-reproducibility.

References

1. Abbott, N.J., L. Rönnbäck, and E. Hansson, *Astrocyte–endothelial interactions at the blood–brain barrier.* Nature Reviews Neuroscience, 2006. **7**(1): p. 41-53.
2. Begley, D.J. and M.W. Brightman, *Structural and functional aspects of the blood-brain barrier.* Prog Drug Res, 2003. **61**: p. 39-78.
3. Rubin, L.L. and J.M. Staddon, *The cell biology of the blood-brain barrier.* Annu Rev Neurosci, 1999. **22**: p. 11-28.
4. Pardridge, W.M., *Targeting neurotherapeutic agents through the blood-brain barrier.* Arch Neurol, 2002. **59**(1): p. 35-40.
5. Abbott, N.J., *Evidence for bulk flow of brain interstitial fluid: significance for physiology and pathology.* Neurochem Int, 2004. **45**(4): p. 545-52.
6. Reese, T.S. and M.J. Karnovsky, *Fine structural localization of a blood-brain barrier to exogenous peroxidase.* J Cell Biol, 1967. **34**(1): p. 207-17.
7. Pardridge, W.M., *Drug Delivery to the Brain.* J Cereb Blood Flow Metab, 1997. **17**(7): p. 713-731.
8. Ridet, J.L., et al., *Reactive astrocytes: cellular and molecular cues to biological function.* Trends Neurosci, 1997. **20**(12): p. 570-7.
9. Furuse, M., et al., *Occludin: a novel integral membrane protein localizing at tight junctions.* J Cell Biol, 1993. **123**(6 Pt 2): p. 1777-88.
10. Suzuki, H., Terasaki, T., and Sugiyama, Y., Adv. Drug. Deliv. Rev., 1997. **25**: p. 257-285.
11. Kusuhara, H. and Y. Sugiyama, *Efflux transport systems for drugs at the blood-brain barrier and blood-cerebrospinal fluid barrier (Part 2).* Drug Discov Today, 2001. **6**(4): p. 206-212.
12. Lee, G., et al., *Drug transporters in the central nervous system: brain barriers and brain parenchyma considerations.* Pharmacol Rev, 2001. **53**(4): p. 569-96.
13. Schlageter, K.E., et al., *Microvessel organization and structure in experimental brain tumors: microvessel populations with distinctive structural and functional properties.* Microvasc Res, 1999. **58**(3): p. 312-28.
14. Rowland LP, F.M., Rubin LL, *Cerebrospinal fluid: blood-brain barrier, brain oedema and hydrocephalus.* Principles of Neural Science, ed., 1992: p. 11.
15. Schwaninger, M., et al., *Bradykinin induces interleukin-6 expression in astrocytes through activation of nuclear factor-kappaB.* J Neurochem, 1999. **73**(4): p. 1461-6.
16. Tsuji, A. and I.I. Tamai, *Carrier-mediated or specialized transport of drugs across the blood-brain barrier.* Adv Drug Deliv Rev, 1999. **36**(2-3): p. 277-290.
17. Pardridge, W.M., *Blood-brain barrier delivery.* Drug Discov Today, 2007. **12**(1-2): p. 54-61.
18. Schinkel, A.H., *P-Glycoprotein, a gatekeeper in the blood-brain barrier.* Adv Drug Deliv Rev, 1999. **36**(2-3): p. 179-194.
19. Pardridge, W.M., *The blood-brain barrier: bottleneck in brain drug development.* NeuroRx, 2005. **2**(1): p. 3-14.
20. Pao, S.S., I.T. Paulsen, and M.H. Saier, Jr., *Major facilitator superfamily.* Microbiol Mol Biol Rev, 1998. **62**(1): p. 1-34.

21. Westholm, D.E., et al., *Evidence of Evolutionary Conservation of Function between the Thyroxine Transporter Oatp1c1 and Major Facilitator Superfamily Members.* Endocrinology, 2010.
22. Hediger, M.A., et al., *The ABCs of solute carriers: physiological, pathological and therapeutic implications of human membrane transport proteinsIntroduction.* Pflugers Arch, 2004. **447**(5): p. 465-8.
23. Hagenbuch, B. and P.J. Meier, *The superfamily of organic anion transporting polypeptides.* Biochim Biophys Acta, 2003. **1609**(1): p. 1-18.
24. Hagenbuch, B. and P.J. Meier, *Organic anion transporting polypeptides of the OATP/ SLC21 family: phylogenetic classification as OATP/ SLCO superfamily, new nomenclature and molecular/functional properties.* Pflugers Arch, 2004. **447**(5): p. 653-65.
25. Fujiwara, K., et al., *Identification of thyroid hormone transporters in humans: different molecules are involved in a tissue-specific manner.* Endocrinology, 2001. **142**(5): p. 2005-12.
26. Abe, T., et al., *Identification of a novel gene family encoding human liver-specific organic anion transporter LST-1.* J Biol Chem, 1999. **274**(24): p. 17159-63.
27. Kullak-Ublick, G.A., et al., *Organic anion-transporting polypeptide B (OATP-B) and its functional comparison with three other OATPs of human liver.* Gastroenterology, 2001. **120**(2): p. 525-33.
28. Pizzagalli, F., et al., *Identification of a novel human organic anion transporting polypeptide as a high affinity thyroxine transporter.* Mol Endocrinol, 2002. **16**(10): p. 2283-96.
29. Mikkaichi, T., et al., *Isolation and characterization of a digoxin transporter and its rat homologue expressed in the kidney.* Proc Natl Acad Sci U S A, 2004. **101**(10): p. 3569-74.
30. Kullak-Ublick, G.A., et al., *Molecular and functional characterization of an organic anion transporting polypeptide cloned from human liver.* Gastroenterology, 1995. **109**(4): p. 1274-82.
31. Gao, B., et al., *Organic anion-transporting polypeptides mediate transport of opioid peptides across blood-brain barrier.* J Pharmacol Exp Ther, 2000. **294**(1): p. 73-9.
32. Hagenbuch, B., B. Gao, and P.J. Meier, *Transport of xenobiotics across the blood-brain barrier.* News Physiol Sci, 2002. **17**: p. 231-4.
33. Fischer, W.J., et al., *Organic anion transporting polypeptides expressed in liver and brain mediate uptake of microcystin.* Toxicol Appl Pharmacol, 2005. **203**(3): p. 257-63.
34. Kullak-Ublick, G.A., et al., *Dehydroepiandrosterone sulfate (DHEAS): identification of a carrier protein in human liver and brain.* FEBS Lett, 1998. **424**(3): p. 173-6.
35. Steckelbroeck, S., et al., *Steroid sulfatase (STS) expression in the human temporal lobe: enzyme activity, mRNA expression and immunohistochemistry study.* J Neurochem, 2004. **89**(2): p. 403-17.

36. Lee, W., et al., *Polymorphisms in human organic anion-transporting polypeptide 1A2 (OATP1A2): implications for altered drug disposition and central nervous system drug entry.* J Biol Chem, 2005. **280**(10): p. 9610-7.
37. Maeda, T., et al., *Identification of influx transporter for the quinolone antibacterial agent levofloxacin.* Mol Pharm, 2007. **4**(1): p. 85-94.
38. Fujino, H., et al., *Transporter-mediated influx and efflux mechanisms of pitavastatin, a new inhibitor of HMG-CoA reductase.* J Pharm Pharmacol, 2005. **57**(10): p. 1305-11.
39. Ho, R.H., et al., *Drug and bile acid transporters in rosuvastatin hepatic uptake: function, expression, and pharmacogenetics.* Gastroenterology, 2006. **130**(6): p. 1793-806.
40. van Montfoort, J.E., et al., *Functional characterization of the mouse organic-anion-transporting polypeptide 2.* Biochim Biophys Acta, 2002. **1564**(1): p. 183-8.
41. Su, Y., X. Zhang, and P.J. Sinko, *Human organic anion-transporting polypeptide OATP-A (SLC21A3) acts in concert with P-glycoprotein and multidrug resistance protein 2 in the vectorial transport of Saquinavir in Hep G2 cells.* Mol Pharm, 2004. **1**(1): p. 49-56.
42. Badagnani, I., et al., *Interaction of methotrexate with organic-anion transporting polypeptide 1A2 and its genetic variants.* J Pharmacol Exp Ther, 2006. **318**(2): p. 521-9.
43. van der Deure, W.M., R.P. Peeters, and T.J. Visser, *Molecular aspects of thyroid hormone transporters, including MCT8, MCT10, and OATPs, and the effects of genetic variation in these transporters.* J Mol Endocrinol, 2010. **44**(1): p. 1-11.
44. Gao, B., et al., *Localization of organic anion transporting polypeptides in the rat and human ciliary body epithelium.* Exp Eye Res, 2005. **80**(1): p. 61-72.
45. Sugiyama, D., et al., *Functional characterization of rat brain-specific organic anion transporter (Oatp14) at the blood-brain barrier: high affinity transporter for thyroxine.* J Biol Chem, 2003. **278**(44): p. 43489-95.
46. Tohyama, K., H. Kusuhara, and Y. Sugiyama, *Involvement of multispecific organic anion transporter, Oatp14 (Slc21a14), in the transport of thyroxine across the blood-brain barrier.* Endocrinology, 2004. **145**(9): p. 4384-91.
47. Kullak-Ublick, G.A., et al., *Hepatic transport of bile salts.* Semin Liver Dis, 2000. **20**(3): p. 273-92.
48. Gerd, A.K.-U., et al., *Organic anion-transporting polypeptide B (OATP-B) and its functional comparison with three other OATPs of human liver.* Gastroenterology, 2001. **120**(2): p. 525-533.
49. Sugiyama, D., et al., *Involvement of multidrug resistance associated protein 1 (Mrp1) in the efflux transport of 17beta estradiol-D-17beta-glucuronide (E217betaG) across the blood-brain barrier.* Pharm Res, 2003. **20**(9): p. 1394-400.
50. Westholm, D.E., et al., *Competitive inhibition of organic anion transporting polypeptide 1c1-mediated thyroxine transport by the fenamate class of nonsteroidal antiinflammatory drugs.* Endocrinology, 2009. **150**(2): p. 1025-32.

51. Li, J.Y., R.J. Boado, and W.M. Pardridge, *Blood-brain barrier genomics.* J Cereb Blood Flow Metab, 2001. **21**(1): p. 61-8.
52. Sugiyama, D., et al., *Effect of 17 beta-estradiol-D-17 beta-glucuronide on the rat organic anion transporting polypeptide 2-mediated transport differs depending on substrates.* Drug Metab Dispos, 2002. **30**(2): p. 220-3.
53. Westholm, D.E., et al., *The blood-brain barrier thyroxine transporter organic anion-transporting polypeptide 1c1 displays atypical transport kinetics.* Endocrinology, 2009. **150**(11): p. 5153-62.
54. Noe, J., et al., *Substrate-dependent drug-drug interactions between gemfibrozil, fluvastatin and other organic anion-transporting peptide (OATP) substrates on OATP1B1, OATP2B1, and OATP1B3.* Drug Metab Dispos, 2007. **35**(8): p. 1308-14.
55. Tamai, I., et al., *Functional characterization of human organic anion transporting polypeptide B (OATP-B) in comparison with liver-specific OATP-C.* Pharm Res, 2001. **18**(9): p. 1262-9.
56. Grube, M., et al., *Organic anion transporting polypeptide 2B1 is a high-affinity transporter for atorvastatin and is expressed in the human heart.* Clin Pharmacol Ther, 2006. **80**(6): p. 607-20.
57. Gui, C., et al., *Effect of pregnane X receptor ligands on transport mediated by human OATP1B1 and OATP1B3.* Eur J Pharmacol, 2008. **584**(1): p. 57-65.
58. Hakes, D.J. and R. Berezney, *Molecular cloning of matrin F/G: A DNA binding protein of the nuclear matrix that contains putative zinc finger motifs.* Proc Natl Acad Sci U S A, 1991. **88**(14): p. 6186-90.
59. Schiffer, M., C.H. Chang, and F.J. Stevens, *The functions of tryptophan residues in membrane proteins.* Protein Eng, 1992. **5**(3): p. 213-4.
60. Hagenbuch, B. and C. Gui, *Xenobiotic transporters of the human organic anion transporting polypeptides (OATP) family.* Xenobiotica, 2008. **38**(7-8): p. 778-801.
61. Hartley, J.L., G.F. Temple, and M.A. Brasch, *DNA cloning using in vitro site-specific recombination.* Genome Res, 2000. **10**(11): p. 1788-95.
62. Miyagawa, M., et al., *The eighth and ninth transmembrane domains in organic anion transporting polypeptide 1B1 affect the transport kinetics of estrone-3-sulfate and estradiol-17beta-D-glucuronide.* J Pharmacol Exp Ther, 2009. **329**(2): p. 551-7.